

Random Matrix Theory and Chiral Symmetry in QCD

J.J.M. Verbaarschot

Department of Physics and Astronomy, SUNY, Stony Brook, NY 11794-3800

T. Wettig

Department of Physics, Yale University, New Haven, CT 06520-8120 and
RIKEN BNL Research Center, Brookhaven National Laboratory, Upton, NY 11973-5000

KEYWORDS: effective low energy theories, finite volume partition function, lattice QCD

ABSTRACT: Random matrix theory is a powerful way to describe universal correlations of eigenvalues of complex systems. It also may serve as a schematic model for disorder in quantum systems. In this review, we discuss both types of applications of chiral random matrix theory to the QCD partition function. We show that constraints imposed by chiral symmetry and its spontaneous breaking determine the structure of low-energy effective partition functions for the Dirac spectrum. We thus derive exact results for the low-lying eigenvalues of the QCD Dirac operator. We argue that the statistical properties of these eigenvalues are universal and can be described by a random matrix theory with the global symmetries of the QCD partition function. The total number of such eigenvalues increases with the square root of the Euclidean four-volume. The spectral density for larger eigenvalues (but still well below a typical hadronic mass scale) also follows from the same low-energy effective partition function. The validity of the random matrix approach has been confirmed by many lattice QCD simulations in a wide parameter range. Stimulated by the success of the chiral random matrix theory in the description of universal properties of the Dirac eigenvalues, the random matrix model is extended to nonzero temperature and chemical potential. In this way we obtain qualitative results for the QCD phase diagram and the spectrum of the QCD Dirac operator. We discuss the nature of the quenched approximation and analyze quenched Dirac spectra at nonzero baryon density in terms of an effective partition function. Relations with other fields are also discussed.

CONTENTS

INTRODUCTION	2
<i>QCD and Chiral Symmetry</i>	2
<i>Random Matrix Theory</i>	6
<i>Effective Low-Energy Theories and Chiral Random Matrix Theory</i>	8
QCD PARTITION FUNCTION AND DIRAC SPECTRUM	9
<i>Basic Definitions</i>	9
<i>Global Symmetries</i>	10
<i>Dirac Spectrum</i>	13
CHIRAL RANDOM MATRIX THEORY	15
<i>Introduction of the Model</i>	15

<i>Sigma Model Representation of Chiral Random Matrix Models</i>	17
<i>θ-Dependence of the Partition Function</i>	18
<i>Spectral Correlation Functions</i>	19
<i>Universality Proofs</i>	22
EFFECTIVE THEORIES AT LOW ENERGIES	23
<i>Finite-Volume Partition Function</i>	23
<i>Leutwyler-Smilga Sum Rules</i>	25
<i>Spectral Mass and Partially Quenched Partition Function</i>	26
<i>Domains of the Partially Quenched Effective Theory</i>	27
<i>QCD in Three Euclidean Dimensions</i>	31
UNIVERSAL PROPERTIES OF THE LATTICE QCD DIRAC SPECTRUM	31
<i>Unfolding</i>	31
<i>Lattice Tests of Chiral Random Matrix Theory</i>	32
<i>The Thouless Energy and Beyond</i>	37
SCHEMATIC MODELS	38
<i>Chiral Random Matrix Models for the Chiral Phase Transition at Nonzero Temperature</i>	39
<i>Chiral Random Matrix Models at Nonzero Chemical Potential</i>	41
<i>Phase Diagram for the QCD Partition Function</i>	46
<i>Random Matrix Triality at $\mu \neq 0$</i>	48
RELATED MODELS AND RELATIONS TO OTHER FIELDS	50
<i>One-Plaquette Models of Lattice QCD</i>	50
<i>Universal Conductance Fluctuations in Disordered Mesoscopic Systems</i>	51
<i>Anderson Localization</i>	51
<i>Non-Hermitian Models with Disorder</i>	52
<i>Andreev Scattering</i>	53
<i>Mathematical Physics and Quantum Gravity</i>	53
CONCLUSIONS	54

1 INTRODUCTION

Well before the advent of quantum chromodynamics (QCD), the theory of the strong force, it was realized that the essential ingredients of the hadronic world at low energies are chiral symmetry and its spontaneous breaking. (see e.g. Refs. [1, 2]). Mainly through lattice QCD simulations, it has become well established that chiral symmetry breaking by the vacuum state of QCD is a nonperturbative phenomenon that results from the interaction of many microscopic degrees of freedom. We argue in this review that the complexity of the QCD vacuum leads to a low-energy description that is completely dictated by the global symmetries of QCD. This interpretation of Goldstone's theorem provides a natural duality between a strongly interacting fundamental theory and a weakly interacting low-energy effective theory.

1.1 QCD and Chiral Symmetry

We illustrate the concept of spontaneous symmetry breaking using the simpler example of a classical spin system with two rotational degrees of freedom. The Hamiltonian of this system has a certain symmetry: It is invariant under rotations. In mathematical language, the symmetry group is $G = O(3)$. However, at low temperatures, the ground state of the system does not exhibit this sym-

metry. In a small external magnetic field, which breaks the rotational invariance explicitly, the spins will polarize in the direction of the magnetic field. In the thermodynamic limit, the spins remain polarized even if the magnetic field is switched off completely. This phenomenon is known as spontaneous magnetization. The ground state is no longer invariant under $O(3)$ rotations but only under $O(2)$ rotations in the plane perpendicular to the spontaneous magnetization. In mathematical language, the full symmetry group $G = O(3)$ is spontaneously broken to a smaller symmetry group $H = O(2)$. The spontaneously broken phase is characterized by low-energy excitations in the form of spin waves in the plane perpendicular to the spontaneous magnetization. This is a consequence of a general theorem known as Goldstone's theorem [3], which tells us that spontaneous breaking of a continuous symmetry leads to low-lying excitations, the Goldstone modes, with a mass that vanishes in the absence of a symmetry-breaking field.

The Goldstone modes are given by the fluctuations in the plane perpendicular to the direction of the spontaneous magnetization. Thus, the spin system has two Goldstone modes. In general, spontaneous symmetry breaking in a system of spins with n components is associated with $n - 1$ Goldstone modes. This number is also equal to the number of generators of the coset G/H [the number of generators of $O(n)$ is $n(n - 1)/2$].

A spontaneously broken symmetry is characterized by an order parameter, which in this case is the spontaneous magnetization. At nonzero temperature, the alignment of the spins is counteracted by their thermal motion, and above a critical temperature (the Curie temperature) the spontaneous magnetization vanishes.

Let us now consider the hadronic world and interpret the particle spectrum in terms of the concepts discussed above. We will look for the simplest theory consistent with the following two empirical facts: (a) there are three bosonic particles, the pions, that are much lighter than all other hadrons and (b) the proton and the neutron have almost the same mass. Fact (a) implies that there are three Goldstone bosons associated with a spontaneously broken symmetry. Assume that the underlying theory is based on an n -component field without preferred directions, i.e. the theory is invariant under $O(n)$ transformations of the fields. Spontaneous symmetry breaking means that the ground state has a preferred direction, leaving $n - 1$ directions for the Goldstone modes. Since there are three pions, this suggests that $n = 4$ and that the ground state of the theory should be symmetric under $O(3)$. The $O(3)$ symmetry is the familiar isospin symmetry, which results in the near equality of the masses of the pions and of the mass of the proton and the neutron, fact (b). As was first conjectured by Gell-Mann and Lévy [1], the theory of the strong force is based on an $O(4)$ invariance spontaneously broken to $O(3)$ with nucleons transforming according to $SU(2)$. This is the familiar linear σ -model. Since the pions are not completely massless, a small $O(4)$ symmetry-breaking mass term should also be present in the theory.

The σ -model is a phenomenological model for the interactions of pions and nucleons. It has been very successful in explaining many previously known empirical relations. Our aim, however, is to understand chiral symmetry in terms of QCD, the fundamental theory of the strong interactions. Quantum chromodynamics is a gauge theory of quarks that come in six different flavors and three different colors. The gauge field interaction is according to the non-Abelian $SU(3)$ color group. Two of the six quarks are nearly massless, and at low energies QCD is

well approximated by a theory with only the two lightest quarks. They are mixed by the $SU(2)$ isospin symmetry group. This symmetry is exact for degenerate quark masses. For massless quarks, there is an additional symmetry. The helicity of a particle is a good quantum number, and the right-handed and left-handed quarks can be rotated independently. The isospin or vector symmetry rotates both chiralities in the same way whereas the axial $SU(2)$ group rotates them in the opposite direction. This explains that the chiral symmetry group in the massless case is $G = SU(2) \times SU(2)$, which is isomorphic to $O(4)$. The mass term breaks this symmetry explicitly and thus plays the role of the magnetic field in the spin system. Even in the massless case, however, the vacuum state of QCD is characterized by a nonzero expectation value of the chiral condensate, which, like the mass term, mixes right-handed and left-handed quarks. Thus, in the vacuum, the axial part of the symmetry group G is broken spontaneously. The ground state is not unique, and the degenerate states are connected by the broken group G . The degeneracy can be lifted by means of a small mass term, and in the thermodynamic limit the system will be frozen in this direction, i.e. the direction of the QCD vacuum state is determined by the mass term. This is exactly the same situation as in the spin system discussed above. The Goldstone modes analogous to spin waves are the pions, with a mass that is well below the typical hadronic mass scale of about 1 GeV. As in the spin system, we expect that the expectation value of the chiral condensate will become zero above a critical temperature. This phenomenon is known as the restoration of chiral symmetry. The chirally symmetric phase probably existed in the early universe and may be produced in relativistic heavy-ion collisions.

Although QCD is the consistent theory of the strong interactions, many questions remain unanswered. For example, why have its constituents never been observed in nature? This phenomenon is known as confinement and means that all physical states are color singlets. QCD is best understood at high energies, where, because of asymptotic freedom, quarks and gluons become weakly interacting and perturbative calculations are possible. At low energies, on the other hand, it is necessary to rely on nonperturbative approaches. One approach is to study the QCD partition function by means of Monte Carlo simulations of a discretized version of the QCD action. This approach has been very fruitful, and a great deal of our understanding of low-energy QCD is based on such calculations (for a recent review, see Ref. [4]). The drawback is that large-scale simulations do not necessarily provide a simple picture of the relevant degrees of freedom. Therefore, it is often advantageous to study QCD by means of effective models or theories. One example is the instanton liquid vacuum [5], which is a model for an ensemble of relevant gauge field configurations. Effective low-energy theories are a second example. We already mentioned the σ -model for pions and nucleons. However, because of the spontaneous breaking of chiral symmetry and the existence of a mass gap in QCD, one can do better. Based on chiral symmetry one can formulate an exact low-energy theory for the Goldstone modes. This nonlinear σ -model is the basis for a systematic low-energy expansion [6, 7] that is discussed in detail in Secs. 1.3 and 4.

The QCD partition function can be written as a Euclidean path integral that can be expressed as the expectation value of the fermion determinant,

$$Z = \left\langle \prod_f \det(\mathcal{D} + m_f) \right\rangle. \quad (1)$$

Here the average is over all gauge fields weighted by the Euclidean Yang-Mills action, the product is over quark flavors of mass m_f , and \mathcal{D} is the Dirac operator, which we introduce in great detail in Sec. 2. The fermion determinant can be expressed as a product over the eigenvalues $i\lambda_n$ of the Dirac operator. Therefore, we may also interpret the average as an average over the eigenvalues with probability distribution determined by the gauge field dynamics. We have argued that spontaneous breaking of chiral symmetry means that a small quark mass leads to a macroscopic realignment of the QCD vacuum. It is clear from the QCD partition function that this is only possible if there is an accumulation of Dirac eigenvalues near zero. Otherwise, a small mass term would be completely dominated by the much larger eigenvalues in the factors of $(i\lambda_n + m_f)$. For a free Dirac operator in a four-dimensional box, the eigenvalue density is proportional to λ^3 and thus vanishes near zero. Therefore, the small eigenvalues must be due to interactions mediated by the gauge fields.

There are two possibilities. First, the eigenvalues may originate from the exactly zero Dirac eigenvalues in the field of an instanton. At a nonzero density of the liquid of instantons and anti-instantons, the zero eigenvalues are distributed over a band because of interactions that lift the degeneracy of the eigenvalues [8]. The eigenvalue repulsion results in a nonzero eigenvalue density near zero. Second, the eigenvalues may originate from the bulk of the Dirac spectrum. As is the case for any interaction in quantum mechanics, the interactions mediated by the gauge fields lead to a repulsion of the eigenvalues. For increasing interaction strength, it is then advantageous for the eigenvalues to move to a region with a low eigenvalue density. Both mechanisms of spontaneous chiral symmetry breaking rely on the repulsion of eigenvalues in interacting systems. This topic has been investigated in detail by means of random matrix theory, discussed in the next subsection.

As mentioned above, we expect chiral symmetry to be restored at high temperatures [9]. This is confirmed by lattice QCD simulations, which show a critical temperature of about 150 MeV [10]. However, there is another direction in which the QCD partition function can be explored, namely at nonzero baryon number density. In this domain, rigorous results are available only at infinite baryon number density [11]. This raises the question to what extent these results can be extrapolated to physically interesting densities. Because of the complex phase of the fermion determinant, Monte Carlo simulations are not possible in this case. Therefore, it is not surprising that many of the recent developments in QCD at nonzero density are based on the analysis of effective models [12, 13]. The picture that has emerged for two massless flavors is that a first-order chiral phase transition occurs at zero temperature along the chemical potential axis. Renormalization-group arguments and lattice QCD simulations indicate that for two massless flavors, a second-order phase transition occurs at zero chemical potential along the temperature axis. The expectation is that a line of first-order transitions and a line of second-order transitions will extend in the μT plane and will join at the tricritical point, as indicated in Fig. 1. A color-superconducting phase is conjectured to exist at higher densities [12, 13, 11] but the discussion of this phase is beyond the scope of this review. One of the questions we address is the robustness of this picture based on the dynamics of the eigenvalues of the QCD Dirac operator.

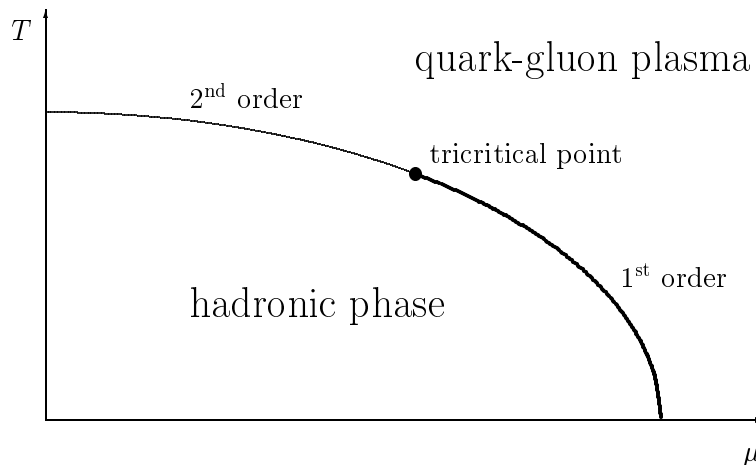


Figure 1: A minimal phase diagram for QCD with two massless flavors at nonzero temperature and density.

1.2 Random Matrix Theory

Random matrix theory (RMT) first appeared in the mathematical literature in 1928 [14] and was first applied to physics in the context of nuclear resonances by Wigner almost 50 years ago [15]. At that time, theoretical approaches such as the shell model had been very successful in describing the low-lying excitations of complex nuclei. However, highly excited resonances, which can be observed experimentally by neutron scattering, could not be described by the microscopic theory. The problem is generic: For any complex quantum system containing many degrees of freedom with complicated dynamics, it is very hard, if not impossible, to obtain exact results for the energy levels far above the ground state of the system.

Having acknowledged that the highly excited states cannot be predicted individually, one can ask whether the experimental data have some generic statistical features that can be described theoretically. This is where RMT comes in. Every quantum system is described by a Hamilton operator that can be expressed in matrix form. For a complex quantum system such as a large nucleus, this matrix is very complicated, and we may not even know its details. In this case, one approach is to assume that all interactions that are consistent with the symmetries of the system are equally likely. This means replacing the elements of the Hamilton matrix by random numbers that are uncorrelated and distributed according to the same probability distribution. To obtain definite results, observables such as the level density must then be averaged over the random matrix elements. This defines a statistical theory of energy levels, which is mathematically known as RMT. An important point is that the random matrix must have the same symmetries as the original Hamilton matrix. A collection of early papers on RMT can be found in the book by Porter [16], and the standard reference on RMT is the book by Mehta [17].

Can such an enormous simplification of the real problem describe empirical data? A similar puzzle occurred in the theory of critical phenomena, in which the critical behavior does not depend on the detailed dynamics of the theory. The

reason for this simplification is the appearance of a length scale, the correlation length, that diverges at the critical point. Because of the corresponding separation of scales, it is possible to integrate out the short-wavelength fluctuations and renormalize the theory to a fixed-point theory that does not depend on the details of the initial theory. What is the separation of scales that takes place in quantum spectra? The two basic scales are the average level spacing and the scale of the variation of the average level spacing. The equivalent of the correlation length is the inverse average level spacing, which diverges in the thermodynamic limit or the semiclassical limit. We thus expect that spectral properties on the scale of the average level spacing do not depend on the details of the underlying dynamics. They are universal.

Universal properties can be studied in the simplest model of a given universality class and, in this way, exact analytical results for the correlation functions can be obtained. In the case of spectral correlations the simplest models of the universality classes are the Gaussian RMTs, and in the past three decades many exact results have been derived for these models. Unfortunately, in most cases it is not possible to prove whether a given theory belongs to one of the RMT universality classes. Therefore, random matrix predictions are usually verified by comparisons with empirical data.

Since Wigner's original proposal, universal quantities have been identified and computed in a variety of fields including nuclear physics, atomic and molecular physics, disordered mesoscopic systems, quantum systems with classically chaotic analogs, two-dimensional quantum gravity, conformal field theory, and QCD. A recent comprehensive review of the applications of RMT can be found in Ref. [18]. RMT is now an independent subfield of mathematical physics. It provides a unifying description of universal statistical features of many different quantum systems and is applicable whenever a system is sufficiently complex.

Let us raise an interesting point here. The eigenvalues of the Hamilton matrix for a given quantum system are the quantities of primary interest. Instead of going through RMT to compute the eigenvalues, an alternative — and much simpler — approach might be to postulate random eigenvalues. It turns out that this does not describe empirical data, at least not if the random eigenvalues are uncorrelated. Therefore, in addition, one would have to postulate how the eigenvalues are correlated, and it is not at all clear how to do this. In RMT, on the other hand, one starts with uncorrelated random matrix elements. At the end of the calculation, one finds that the resulting eigenvalues are strongly correlated in precisely the right way to describe the data.

In most applications, RMT is used to describe the statistics of energy levels, i.e. of the eigenvalues of the Hamilton operator. For the Euclidean QCD partition function, it is more natural to construct a random matrix model for the Dirac operator. As shown in the previous subsection, the spectrum of this operator is intimately related to the phenomenon of chiral symmetry breaking. This establishes the connection between RMT and chiral symmetry announced in the title of this review. We use random matrix methods to study the Dirac spectrum and its implications for chiral symmetry breaking.

It is important to note that RMT can only provide an exact description of universal quantities. It cannot be used for the calculation of nonuniversal observables such as the average level spacing. Such behavior is well known in statistical mechanics where, for example, the Ising model describes the critical exponents of the liquid-gas phase transition but does not give the critical temperature. In the case

of the distribution of the eigenvalues of a system, the global spectral density is not described by RMT. For example, for the Gaussian random matrix ensembles the average spectral density is a semicircle, whereas in real systems it typically increases strongly with excitation energy. In contrast, universal quantities do not depend on the details of the dynamics of the system. In RMT, they do not depend on the distribution of the random matrix elements. It is crucial to distinguish the universal quantities from the model-dependent ones. In the first five sections of this review, we mainly concentrate on the universal, model-independent features that yield exact quantitative results. However, it is sometimes useful to construct random matrix models to obtain a qualitative description of the physics in a disordered system. As we show in Sec. 6, schematic random matrix models for QCD at nonzero temperature and density can yield important qualitative insights into problems that are otherwise difficult to tackle.

1.3 *Effective Low-Energy Theories and Chiral Random Matrix Theory*

Let us now make the connection between QCD, effective low-energy theories for QCD, and chiral RMT. We concentrate here on the big picture, postponing a more detailed discussion to Secs. 3 and 4.

At low energies, quarks and gluons are confined in hadrons, i.e. the particles we observe in nature are composite objects. Instead of attempting to describe the results of low-energy scattering experiments in terms of quarks and gluons, it is often simpler to use an effective theory whose elementary degrees of freedom are the lightest particles of the theory. As mentioned earlier, in QCD the low-lying degrees of freedom are the pions resulting from the spontaneous breaking of chiral symmetry. Therefore, an essential ingredient in the construction of the effective low-energy theory is the requirement that it correctly incorporates the chiral symmetries of the original theory. Since the up- and down-quark are not completely massless in nature, the pions are not massless but have a small mass of about 140 MeV. They are much lighter than the lightest non-Goldstone particles, such as the ρ -meson or the nucleons, which have a mass of about $\Lambda \sim 1$ GeV. This means that at sufficiently low energies, the QCD partition function is well approximated by the partition function of an effective low-energy theory involving only pions.

We now consider QCD in a finite Euclidean volume $V_4 = L^4$. The partition function is then dominated by the pions if

$$\frac{1}{\Lambda} \ll L. \quad (2)$$

This statement follows from Eq. (4) below by comparing the contribution of the pion, $\exp(-m_\pi L)$, to that of a heavier particle, $\exp(-\Lambda L)$. The interactions of the pions are described by an effective chiral Lagrangian that will be given in Sec. 4. The fields in this Lagrangian can be separated into zero-momentum modes (constant fields) and nonzero-momentum modes. It was realized by Gasser and Leutwyler [19] that there exists a kinematic regime where the fluctuations of the zero-momentum modes dominate the fluctuations of the nonzero-momentum modes. This regime is given by the condition

$$L \ll \frac{1}{m_\pi}, \quad (3)$$

where m_π is the pion mass. Intuitively, this means that the wavelength of the pion is much larger than the linear extent of the box. Thus, the pion field does not vary appreciably over the size of the box, so the derivative terms are small. (These statements are quantified in Sec. 4.) We need consider only the zero-momentum modes in the regime of Eq. (3). For constant fields, the spacetime integral in the action can be replaced by the four-volume, and, effectively, we only have to deal with a much simpler zero-dimensional theory. However, the global symmetries remain important.

We are now ready to make the connection to chiral RMT. A random matrix, as introduced in the previous subsection, contains independently distributed random variables. Each element of the matrix has the same average size. On the other hand, the matrix elements of the Dirac operator contain specific correlations due to the gauge fields and the kinetic terms, which are not included in the RMT. Only the global symmetries of QCD are included in the RMT. Since the random matrix elements do not have any spacetime dependence, we expect that in the domain of Eq. (3), which is dominated by constant fields, the RMT reproduces the mass dependence of the finite-volume partition function.

To summarize, the three ingredients in the construction of the finite-volume effective theory from QCD in the regime of Eq. (3) are the following: (a) the global symmetries of QCD, (b) the spontaneous breaking of chiral symmetry, and (c) the fact that the partition function is dominated by the constant Goldstone fields. There is an almost one-to-one correspondence to the properties of the chiral random matrix model [20]: (a) the Dirac matrix is replaced by a random matrix with the same global symmetries, (b) chiral symmetry is broken spontaneously in the limit of infinitely large random matrices, and (c) the random matrix elements do not have any spacetime dependence.

2 QCD PARTITION FUNCTION AND DIRAC SPECTRUM

After the introductory remarks on our basic philosophy in Sec. 1, we now present a detailed discussion of the properties of the QCD partition function and the Dirac operator.

2.1 Basic Definitions

The QCD partition function is defined as

$$Z^{\text{QCD}} = \text{Tr} e^{-\beta H} , \quad (4)$$

where β is the inverse temperature and H is the QCD Hamiltonian in a box of volume $V_3 = L^3$. It can be rewritten as a (suitably regularized) functional integral in Euclidean space,

$$Z^{\text{QCD}} = \int DA_\mu \prod_{f=1}^{N_f} \det(\mathcal{D} + m_f) e^{-S_{\text{YM}}} , \quad (5)$$

where N_f is the number of quark flavors and S_{YM} is the Euclidean Yang-Mills action. The Euclidean four-volume is $V_4 = V_3\beta$. The A_μ are non-Abelian gauge fields, which can be represented as

$$A_\mu = A_\mu^a \frac{T_a}{2} , \quad (6)$$

where the T_a are the generators of the gauge group $SU(N_c)$. The number of colors is denoted by N_c . The QCD Dirac operator is given by

$$\mathcal{D} = \gamma_\mu(\partial_\mu + iA_\mu). \quad (7)$$

This operator is anti-Hermitian, $\mathcal{D}^\dagger = -\mathcal{D}$. The γ_μ are Euclidean gamma matrices with $\{\gamma_\mu, \gamma_\nu\} = 2\delta_{\mu\nu}$. We use the chiral representation in which $\gamma_5 \equiv \gamma_1\gamma_2\gamma_3\gamma_4 = \text{diag}(1, 1, -1, -1)$.

2.2 Global Symmetries

The structure of the QCD Lagrangian is to a large extent determined by symmetries and renormalizability. As noted above, it is important to analyze these symmetries to construct the correct effective low-energy theory and the correct random matrix model. We now discuss three important global symmetries of the partition function and the Dirac operator.

2.2.1 CHIRAL SYMMETRY AND TOPOLOGY

The Dirac operator satisfies

$$\{\gamma_5, \mathcal{D}\} = 0. \quad (8)$$

This relation is a compact expression of chiral symmetry, i.e. of the fact that right-handed and left-handed quarks can be rotated independently. One can write down an eigenvalue equation for \mathcal{D} ,

$$\mathcal{D}\psi_n = i\lambda_n\psi_n, \quad (9)$$

where the eigenvalues and eigenfunctions depend on the gauge field in Eq. (7). Using Eq. (8) one can show that the nonzero eigenvalues of \mathcal{D} occur in pairs $\pm i\lambda_n$ with eigenfunctions ψ_n and $\gamma_5\psi_n$. There can also be eigenvalues equal to zero, $\lambda_n = 0$. The corresponding eigenfunctions can be arranged to be simultaneous eigenfunctions of γ_5 with eigenvalue ± 1 , i.e. these states have definite chirality. Denoting the number of zero eigenvalues with positive and negative chirality by N_+ and N_- , respectively, the Atiyah-Singer index theorem states that $\nu \equiv N_+ - N_-$ is a topological invariant that does not change under continuous changes of the gauge field. However, the individual numbers N_+ and N_- are not protected by topology, i.e. very small deformations of the gauge field will lift accidental zero modes. Thus, unless we impose very special constraints on the gauge fields, we generically have either $N_+ = 0$ or $N_- = 0$.

In a chiral basis with $\gamma_5\psi^{R/L} = \pm\psi^{R/L}$, one can use Eq. (8) to show that $\langle\bar{\psi}_m^R|\mathcal{D}|\psi_n^L\rangle = 0 = \langle\bar{\psi}_m^L|\mathcal{D}|\psi_n^R\rangle$ for all m and n , where $\bar{\psi} = \psi^\dagger\gamma_0$. From this property and the fact that \mathcal{D} is anti-Hermitian, it follows that the Dirac operator has the matrix structure

$$\mathcal{D} = \begin{pmatrix} 0 & iW \\ iW^\dagger & 0 \end{pmatrix}. \quad (10)$$

This off-diagonal block structure is characteristic for systems with chiral symmetry. If there are $n + \nu$ right-handed and n left-handed modes, the matrix W has dimension $(n + \nu) \times n$, and the matrix \mathcal{D} in Eq. (10) has $|\nu|$ eigenvalues equal to zero.

The QCD partition function can be decomposed into sectors of definite topological charge ν ,

$$Z^{\text{QCD}}(\theta) = \sum_{\nu=-\infty}^{\infty} e^{i\nu\theta} Z_{\nu}^{\text{QCD}}. \quad (11)$$

Here, the θ -angle is the coefficient of the topological $F\tilde{F}$ term (which violates P and CP conservation) in the Lagrangian. We now show that the θ -dependence of the partition function can be absorbed into the phase of the quark masses. To this end, we introduce complex masses m_f for the right-handed quarks and the complex conjugate masses m_f^* for the left-handed quarks. The partition function then reads

$$Z_{\nu}^{\text{QCD}} = \left\langle \prod_f \hat{m}_f^{|\nu|} \prod_{\lambda_n > 0} (\lambda_n^2 + m_f m_f^*) \right\rangle_{\nu}, \quad (12)$$

where $\hat{m}_f = m_f$ (m_f^*) for $\nu \geq 0$ ($\nu < 0$). In Eq. (12), the average is only over the gauge field configurations with topological charge ν , weighted by the Yang-Mills action. Since

$$e^{i\nu\theta} \prod_f \hat{m}_f^{|\nu|} = \begin{cases} \left(e^{i\theta} \prod_f m_f \right)^{\nu} & \text{for } \nu \geq 0 \\ \left[\left(e^{i\theta} \prod_f m_f \right)^* \right]^{-\nu} & \text{for } \nu < 0, \end{cases} \quad (13)$$

it follows that the θ -dependence of Z^{QCD} is entirely determined by the combination $e^{i\theta} \prod_f m_f$.

2.2.2 FLAVOR SYMMETRIES

The second global symmetry is flavor symmetry, whose spontaneous breaking has profound implications for the hadron spectrum. To make this symmetry explicit, we rewrite the fermion determinant in Z^{QCD} as a Grassmann integral,

$$\prod_{f=1}^{N_f} \det(\mathcal{D} + m_f) = \int d\psi d\bar{\psi} \exp \left[\int d^4x \sum_{f=1}^{N_f} \bar{\psi}_f (\mathcal{D} + m_f) \psi_f \right], \quad (14)$$

where $\bar{\psi} = \psi^\dagger \gamma_0$. Again going to a chiral basis with $\gamma_5 \psi^{R/L} = \pm \psi^{R/L}$, the exponent on the right-hand side of Eq. (14) can be rewritten as

$$\int d^4x \sum_{f=1}^{N_f} \left(\bar{\psi}_f^R i W^\dagger \psi_f^R + \bar{\psi}_f^L i W \psi_f^L + \bar{\psi}_f^R m_f \psi_f^L + \bar{\psi}_f^L m_f \psi_f^R \right). \quad (15)$$

In the chiral limit where all $m_f = 0$, the fermion determinant is invariant under the transformations

$$\begin{aligned} \psi^L &\rightarrow U \psi^L & \bar{\psi}^L &\rightarrow \bar{\psi}^L U^{-1} \\ \bar{\psi}^R &\rightarrow \bar{\psi}^R V^{-1} & \psi^R &\rightarrow V \psi^R. \end{aligned} \quad (16)$$

The only condition on U and V is that their inverses must exist. If the number of right-handed states N_R is equal to the number of left-handed states N_L , the symmetry is thus¹ $U(N_f) \times U(N_f)$. However, if $N_R \neq N_L$, i.e. if $\nu \neq 0$, the

¹Actually, the symmetry group is $\text{Gl}(N_f) \times \text{Gl}(N_f)$. The restriction to $U(N_f)$ is a consequence of the Riemannian nature of the integration manifold (see Sec. 4.3).

axial symmetry group $U_A(1)$ is broken explicitly by instantons or the anomaly. A second $U(1)$ group, $U_V(1)$, corresponds to the conservation of baryon number. The full flavor symmetry group in the chiral limit is thus given by $G = SU(N_f) \times SU(N_f)$.

If the quark masses are nonzero, the axial $SU(N_f)$ subgroup with $U = V^{-1}$ is broken explicitly by the mass term. The $SU(N_f)$ vector symmetry (with $U = V$) is good for degenerate quark masses ($m_f = m$ for all f) but is broken explicitly for different quark masses ($m_f \neq m_{f'}$ for all $f \neq f'$).

What is much more important than the explicit breaking, however, is the spontaneous breaking of the axial-flavor symmetry. For an axial-flavor-symmetric ground state, the vacuum expectation value $\langle \bar{\psi}\psi \rangle = \langle \bar{\psi}^R\psi^L \rangle + \langle \bar{\psi}^L\psi^R \rangle$ would be zero. However, phenomenological arguments and lattice QCD simulations indicate that $\langle \bar{\psi}\psi \rangle \approx -(240 \text{ MeV})^3$. The spontaneous breaking of the axial symmetry also follows from the absence of parity doublets and the presence of Goldstone bosons, the pions. The quantity $\langle \bar{\psi}\psi \rangle$ is only invariant if $U = V$, i.e. the vacuum state is symmetric under the flavor group $H = SU_V(N_f)$. Thus, the vector symmetries are unbroken whereas the axial symmetries are maximally broken. The first of these statements is in agreement with the Vafa-Witten theorem [21], which states that in vector-like theories such as QCD, vector symmetries cannot be spontaneously broken. The reasons why the axial symmetries are maximally broken [22] are less well understood. The Goldstone manifold is $G/H = SU(N_f)$, and so there are $N_f^2 - 1$ Goldstone bosons.

2.2.3 ANTI-UNITARY SYMMETRIES

Third, we consider the anti-unitary symmetries of the Dirac operator. According to a fundamental theorem by Wigner, a symmetry in quantum mechanics is either unitary or anti-unitary. An anti-unitary symmetry operator A can always be written as $A = UK$, where U is a unitary operator and K is the complex conjugation operator. Below we always consider spectra of an irreducible subspace of the unitary symmetries. If $A = UK$ is an anti-unitary symmetry of the Dirac operator, then the symmetry operator $A^2 = (UK)^2 = UU^*$ is unitary, and in an irreducible subspace it is necessarily a multiple of the identity, $UU^* = \lambda \mathbf{1}$. Because of this relation, U and U^* commute so that λ is real. By unitarity we have $|\lambda| = 1$, which yields $\lambda = \pm 1$. Therefore, the anti-unitary symmetries can be classified according to the sign of A^2 . There are three possibilities for the classification of Hermitian (or anti-Hermitian) operators: (a) there are no anti-unitary symmetries (denoted by the Dyson index $\beta = 2$); (b) if $A^2 = 1$, it is possible to construct a basis in which the operator is real (denoted by the Dyson index $\beta = 1$); (c) if $A^2 = -1$, it is possible to construct a basis in which the matrix elements of the operator can be organized into real (or self-dual) quaternions (denoted by the Dyson index $\beta = 4$).

For QCD with $N_c \geq 3$ and fermions in the fundamental representation of the gauge group, there are no anti-unitary operators that commute with the Dirac operator. This means that the matrix W in Eq. (10) is a general complex matrix with no further symmetries. There are two cases with nontrivial anti-unitary symmetries: QCD with two colors and fermions in the fundamental representation, and QCD with any number of colors and adjoint fermions. We will discuss them next.

For QCD with two colors and fermions in the fundamental representation, the

Dirac operator is given by Eq. (7) with $A_\mu = A_\mu^a \tau_a / 2$, where the τ_a are the SU(2) Pauli matrices in color space. The anti-unitary symmetry in this case is [23, 24]

$$[C\tau_2 K, i\mathcal{D}] = 0, \quad (17)$$

where $C = \gamma_2 \gamma_4$ is the charge conjugation matrix. The square of the anti-unitary operator is $(C\tau_2 K)^2 = 1$. In this case, it is possible to find a basis in which the matrix W in Eq. (10) is real for all gauge field configurations [16].

As a consequence of the pseudoreality of SU(2), the symmetry of the QCD partition function in the chiral limit is enlarged to SU($2N_f$) [22, 25, 26]. An axial U(1) is broken explicitly by instantons or the axial anomaly, as for $N_c \geq 3$. The chiral condensate is only invariant under an Sp($2N_f$) subgroup of SU($2N_f$). The Vafa-Witten theorem, prohibiting the spontaneous breaking of global vector symmetries and assuming maximum breaking of the axial symmetries, thus predicts a pattern of spontaneous chiral symmetry breaking given by SU($2N_f$) \rightarrow Sp($2N_f$). The Goldstone manifold is the coset SU($2N_f$)/Sp($2N_f$), which is the set of antisymmetric unitary matrices. We thus have $2N_f^2 - N_f - 1$ Goldstone bosons [25, 26].

For fermions in the adjoint representation of the gauge group and any number of colors, the Dirac operator is $\mathcal{D}_{ab} = \gamma_\mu (\partial_\mu \delta_{ab} + f_{abc} A_\mu^c)$, where a and b are color indices and the f_{abc} are the structure constants of SU(N_c). In this case, the anti-unitary symmetry is [23, 24]

$$[CK, i\mathcal{D}] = 0. \quad (18)$$

Because of $(CK)^2 = -1$, it follows that the eigenvalues of the Dirac operator are twofold degenerate with linearly independent eigenfunctions. In this case, it is possible to choose a basis in which the matrix elements of W are real (or self-dual) quaternions for all gauge fields. The eigenvalues of such a matrix are unit quaternions and therefore doubly degenerate [27] in the representation of the Dirac matrix as complex numbers.

Restricting ourselves to the case of even N_f , we can show that for N_f Majorana fermions, the flavor symmetry group is now SU(N_f). In this case, the chiral condensate is only invariant under an O(N_f) subgroup of SU(N_f). Applying again the Vafa-Witten theorem with maximum breaking of axial symmetry, we expect the pattern of spontaneous chiral symmetry breaking according to SU(N_f) \rightarrow O(N_f), with the Goldstone manifold given by the coset SU(N_f)/O(N_f). This is the set of symmetric unitary matrices. We thus have $(N_f + 2)(N_f - 1)/2$ Goldstone bosons [25, 26].

On the lattice, the symmetries of the Dirac operator may be different from the continuum symmetries [28]. We return to this point in Sec. 5.2.

2.3 Dirac Spectrum

Based on the eigenvalue equation (9), we define the spectral density of the Dirac operator by

$$\rho(\lambda) = \left\langle \sum_n \delta(\lambda - \lambda_n) \right\rangle, \quad (19)$$

where the average is over gauge fields weighted by the full QCD action. The spectral density is important because of its relation with the order parameter for

spontaneous chiral symmetry breaking, the chiral condensate $\langle \bar{\psi}\psi \rangle$. It was shown by Banks and Casher [29] that

$$\Sigma \equiv |\langle \bar{\psi}\psi \rangle| = \frac{\pi\rho(0)}{V}. \quad (20)$$

To be precise, we should have written $\Sigma = \lim_{\varepsilon \rightarrow 0} \lim_{m \rightarrow 0} \lim_{V \rightarrow \infty} \pi\rho(\varepsilon)/V$, where it is important that the limits are taken in the order indicated. (In the normalization of Eq. (19) the spectral density is proportional to the volume, so the explicit factor of $1/V$ in (20) is canceled to yield a finite result.)

The relation (20) can readily be derived. The chiral condensate is given by

$$\langle \bar{\psi}\psi \rangle = - \lim_{m \rightarrow 0} \lim_{V \rightarrow \infty} \frac{1}{VN_f} \frac{\partial}{\partial m} \log Z^{\text{QCD}}(m). \quad (21)$$

From Eq. (5), this yields

$$\langle \bar{\psi}\psi \rangle = - \lim_{m \rightarrow 0} \lim_{V \rightarrow \infty} \left\langle \frac{1}{V} \sum_n \frac{1}{i\lambda_n + m} \right\rangle. \quad (22)$$

Since the nonzero eigenvalues occur in pairs $\pm i\lambda_n$, their contribution to the sum can be written as $2m/(\lambda_n^2 + m^2)$ (with $\lambda_n > 0$). For gauge fields with topological charge ν , the zero modes contribute a term $|\nu|/(mV)$. Assuming $\langle \nu^2 \rangle \propto V$, we can drop these contributions in the limit $V \rightarrow \infty$. In the same limit, the sum in Eq. (22) can be converted to an integral. In the limit $m \rightarrow 0$, we have $2m/(\lambda^2 + m^2) \rightarrow \pi\delta(\lambda)$, which yields Eq. (20). As discussed above in Sec. 1.1, spontaneous chiral symmetry breaking is encoded in an accumulation of the small Dirac eigenvalues; for the order parameter to be nonzero, we need $\rho(0)/V > 0$.

An immediate consequence of the Banks-Casher relation is that the small eigenvalues are spaced as

$$\Delta\lambda = \frac{1}{\rho(0)} = \frac{\pi}{V\Sigma}, \quad (23)$$

provided that $\rho(0)/V > 0$. This naturally defines a scale

$$z = \lambda V\Sigma \quad (24)$$

for the study of the distribution of individual eigenvalues. For this purpose, it is convenient to define the so-called microscopic spectral density [20]

$$\rho_s(z) = \lim_{V \rightarrow \infty} \frac{1}{V\Sigma} \rho\left(\frac{z}{V\Sigma}\right). \quad (25)$$

This function describes the extreme infrared properties of the Dirac spectrum. Based on the arguments in the introduction, we expect it to be completely determined by the global symmetries of the Dirac operator. As we demonstrate below, $\rho_s(z)$ can be computed both from the low-energy effective theory and from chiral RMT; the results coincide. Further confirmation of these ideas will come from results of lattice QCD simulations.

At this point we would like to add some remarks on possible ultraviolet divergences. As an example, we consider the chiral condensate in the $V \rightarrow \infty$ limit, but before the limit $m \rightarrow 0$ is taken. Converting the sum in Eq. (22) to an integral and dropping the contribution from the zero eigenvalues, we obtain

$$\langle \bar{\psi}\psi \rangle = - \lim_{\Lambda \rightarrow \infty} \lim_{m \rightarrow 0} \int_0^\Lambda d\lambda \frac{2m\rho(\lambda)/V}{\lambda^2 + m^2}, \quad (26)$$

where we have introduced an ultraviolet cutoff Λ that must be removed at the end of the calculation. Asymptotically, the spectral density behaves as $\rho(\lambda) \sim V\lambda^3$, which means that the integral is ultraviolet-divergent. However, this divergence does not contribute to $\langle \bar{\psi}\psi \rangle$ if the $m \rightarrow 0$ limit is taken first to yield the usual Banks-Casher relation. Alternatively, we can first subtract the divergent contributions to the integral (26) and remove the cutoff before taking the chiral limit.

A slightly different situation arises if we consider the dependence of the chiral condensate on a valence (or spectral) mass m_v that does not appear in the average, so that $\rho(\lambda)$ is independent of m_v . The quantity

$$\Sigma(m_v) = \lim_{\Lambda \rightarrow \infty} \int_0^\Lambda d\lambda \frac{2m_v \rho(\lambda)/V}{\lambda^2 + m_v^2} \quad (27)$$

is subject to ultraviolet divergences. Using again the fact that $\rho(\lambda) \sim V\lambda^3$ for large λ , we find that the leading divergence is $\sim m_v \Lambda^2$. If we consider valence masses on the microscopic scale (24) we have $m_v \sim 1/(V\Sigma)$, and if the $V \rightarrow \infty$ limit is taken before the $\Lambda \rightarrow \infty$ limit, the ultraviolet divergences are removed.

In lattice QCD simulations with lattice spacing a , the cutoff is $\Lambda = 1/a$. In the continuum limit, $a \rightarrow 0$, both the coupling constant and the $\bar{\psi}\psi$ -operator have to be renormalized. For a discussion of the ultraviolet divergences in a recent lattice study of $\Sigma(m_v)$ at finite volume, finite quark mass, and finite lattice spacing, see Ref. [30].

3 CHIRAL RANDOM MATRIX THEORY

3.1 Introduction of the Model

In this section we introduce a chiral random matrix theory (chRMT) with the global symmetries of the QCD Dirac operator. In the spirit of the invariant random matrix ensembles, we construct a model with eigenfunctions distributed uniformly over the unitary unit sphere. This is achieved by choosing Gaussian-distributed random matrix elements. We thus arrive at the following chRMT [20, 24]:

$$Z_{N_f, \nu}^\beta(m_1, \dots, m_{N_f}) = \int DW \prod_{f=1}^{N_f} \det(\mathcal{D} + m_f) e^{-\frac{N\beta}{4} \text{Tr } v(W^\dagger W)}, \quad (28)$$

where β is the Dyson index,

$$\mathcal{D} = \begin{pmatrix} 0 & iW \\ iW^\dagger & 0 \end{pmatrix}, \quad (29)$$

and W is an $n \times m$ matrix with $\nu = m - n$ and $N = n + m$. The interpretation of this model is that N low-lying modes interact via a random interaction. A natural representation of this model is in the form of gauge field configurations given by a liquid of instantons. Then the low-lying modes are the zero modes of each instanton. We assume that ν does not exceed \sqrt{N} so that, to a good approximation, $n = N/2$ for large N . The parameter N is identified as the dimensionless volume of spacetime. For the formulation of this model with explicit factors of N/V included, see Ref. [31]. The potential v is defined by

$$v(\phi) = \sum_{k \geq 1} a_k \phi^k. \quad (30)$$

The simplest case is the Gaussian case, where $v(\phi) = \Sigma^2 \phi$. It can be shown (see Sec. 3.5) that the microscopic spectral density does not depend on the higher-order terms in this potential provided that the average spectral density near zero remains nonzero. The matrix elements of W are either real [$\beta = 1$, chiral Gaussian Orthogonal Ensemble (chGOE)], complex [$\beta = 2$, chiral Gaussian Unitary Ensemble (chGUE)], or quaternion real [$\beta = 4$, chiral Gaussian Symplectic Ensemble (chGSE)]. In the latter case, the eigenvalues of \mathcal{D} are doubly degenerate, and the use of Majorana fermions is implemented by replacing the determinant by its square root. For a non-Gaussian potential $v(\phi)$, we will omit the G in the abbreviations and use chOE, chUE, and chSE, respectively. Two earlier attempts to describe QCD Dirac eigenvalues used the Wigner-Dyson ensembles instead of the above chiral ensembles [32].

This model reproduces the following symmetries of the QCD partition function:

- The $U_A(1)$ symmetry. All eigenvalues of the random matrix Dirac operator occur in pairs $\pm i\lambda_n$ or are zero.
- The topological structure of the QCD partition function. The Dirac matrix has exactly $|\nu| = |n - m|$ zero eigenvalues. This identifies ν as the topological sector of the model.
- The flavor symmetry, which is the same as in QCD. For $\beta = 2$ it is $SU(N_f) \times SU(N_f)$, for $\beta = 1$ it is $SU(2N_f)$, and for $\beta = 4$ it is $SU(N_f)$ (each Majorana flavor counts as 1/2 Dirac flavor).
- The chiral symmetry, which is broken spontaneously with a chiral condensate given by

$$\Sigma = \lim_{N \rightarrow \infty} \pi \rho(0) / N . \quad (31)$$

(N is interpreted as the dimensionless volume of spacetime.) The symmetry-breaking pattern is [25] $SU(N_f) \times SU(N_f) \rightarrow SU(N_f)$, $SU(2N_f) \rightarrow Sp(2N_f)$, and $SU(N_f) \rightarrow O(N_f)$ for $\beta = 2, 1$, and 4, respectively — the same as in QCD [22].

- The anti-unitary symmetries. These are implemented by choosing the matrix elements of W to be real, complex, or quaternion real for $\beta = 1$, $\beta = 2$, and $\beta = 4$, respectively.

Along with the invariant random matrix ensembles, the chiral ensembles are part of a larger classification scheme that also includes ensembles for the description of disordered superconductors [33]. In total, 10 different families of random matrix ensembles have been identified. They correspond one-to-one with the Cartan classification of symmetric spaces [34].

The uniform distribution of the eigenfunctions over the unitary unit sphere is expressed as the invariance

$$W \rightarrow U^\dagger W V , \quad (32)$$

where the $n \times n$ matrix U and the $m \times m$ matrix V are orthogonal matrices for $\beta = 1$, unitary matrices for $\beta = 2$, and symplectic matrices for $\beta = 4$. This invariance makes it possible to express the partition function in terms of eigenvalues of W defined by

$$W = U^\dagger \Lambda V . \quad (33)$$

Here, Λ is a diagonal matrix with real diagonal matrix elements $\lambda_k \geq 0$. In terms of the eigenvalues, the partition function (28) is given by

$$Z_{N_f, \nu}^\beta(m_1, \dots, m_{N_f}) = \int d\lambda |\Delta(\lambda^2)|^\beta \prod_k \lambda_k^{\beta|\nu| + \beta - 1} e^{-\frac{N\beta}{4} \nu (\lambda_k^2)} \prod_f m_f^{|\nu|} (\lambda_k^2 + m_f^2), \quad (34)$$

where the Vandermonde determinant is defined by

$$\Delta(\lambda^2) = \prod_{k < l} (\lambda_k^2 - \lambda_l^2). \quad (35)$$

In Eq. (34) and elsewhere in this review, we have omitted the normalization constant of the partition function. From the joint eigenvalue distribution (which is the integrand of Eq. (34)), we see that a nonzero topological charge ν can be introduced by adding $\beta|\nu|/2$ massless flavors to the theory with $\nu = 0$. Therefore, this duality between flavor and topology is a general feature of all correlation functions. For a discussion of this duality in terms of finite volume partition functions, see Refs. [35, 36].

3.2 Sigma Model Representation of Chiral Random Matrix Models

The chiral random matrix partition function can be evaluated using standard random matrix methods. For simplicity, let us consider the case $\beta = 2$. The fermion determinant can be written as a Grassmann integral, and averaging over the Gaussian distribution function results in a four-fermion interaction. Because of the underlying unitary invariance (32) of the chRMT, the fermionic variables only appear in invariant combinations of the form $\sigma^{fg} \sim \bar{\psi}_i^f \psi_i^g$, and the partition function can be rewritten identically in terms of these variables as [20, 37]

$$Z_\nu(m) = \int D\sigma e^{-n\Sigma^2 \text{Tr} \sigma \sigma^\dagger} \det^\nu(\sigma + m\mathbf{1}) \det^n[(\sigma + m\mathbf{1})(\sigma^\dagger + m\mathbf{1})], \quad (36)$$

where the quark masses have been taken real and degenerate for simplicity. The integration is over the real and imaginary parts of the $N_f \times N_f$ arbitrary complex matrix σ . For $m = 0$ this integral is invariant under $\sigma \rightarrow U\sigma V^{-1}$ with U and $V \in \text{SU}(N_f)$. Let us calculate the integrals by a saddle-point approximation. The saddle-point equation reads (notice that $\nu \ll n$)

$$\Sigma^2(\sigma^\dagger + m)\sigma = 1. \quad (37)$$

The condensate at the saddle point is given by

$$|\langle \bar{\psi} \psi \rangle| = \frac{1}{2nN_f} \partial_m \log Z = \frac{\Sigma^2}{2N_f} \langle \text{Tr}(\sigma + \sigma^\dagger) \rangle, \quad (38)$$

where the expectation value is with respect to the partition function (36). The solution of the saddle-point equation, $\bar{\sigma}$, is proportional to the identity matrix. In the chiral limit, we then find $\bar{\sigma} = 1/\Sigma$, and we can identify Σ as the chiral condensate.

The fluctuations about the saddle point can be separated into massive modes with a curvature of order n and Goldstone modes with a curvature of order mn . In the limit $n \rightarrow \infty$, the partition function (36) can be simplified by keeping the

integrals over the Goldstone manifold and performing the remaining integrals by a saddle-point integration. This results in the partition function

$$Z_\nu(m) = \int_{U \in \text{U}(N_f)} DU \det^\nu U e^{n \Sigma \text{Tr} (MU + M^\dagger U^{-1})}, \quad (39)$$

which is the familiar finite volume partition function to be discussed in Sec. 4.1.

3.3 θ -Dependence of the Partition Function

The θ -dependence of the partition function is obtained by summing over all topological sectors of the partition function according to Eq. (11), which applies to full QCD where the partition function is obtained by integrating over the gauge fields. The terms Z_ν in this equation reflect the probability of encountering gauge fields with topological charge ν .

For the effective theory, the partition function in the topological sector ν is given in Eq. (39). However, this ν -dependence is only due to the fermion determinant. In the sum over ν , we should therefore add weight factors $P(\nu)$ that take into account the distribution of topological charge of the quenched gauge fields (i.e. gauge fields generated without the fermion determinant). This yields

$$Z^{\text{eff}}(\theta, m) = \sum_\nu P(\nu) e^{i\nu\theta} Z_\nu^{\text{eff}}(m). \quad (40)$$

Below, we argue that the weight factors can be ignored for light quarks but that they are necessary when one considers the quenched theory (which corresponds to $N_f = 0$ or, equivalently, to the limit of very heavy quarks).

Our starting point is that the topological susceptibility of the quenched gauge fields is nonvanishing, i.e.

$$\frac{\langle \nu^2 \rangle_q}{V} \neq 0. \quad (41)$$

Invoking the central limit theorem, we assume that $P(\nu)$ is Gaussian,

$$P(\nu) = \frac{1}{\sqrt{2\pi \langle \nu^2 \rangle_q}} e^{-\frac{\nu^2}{2 \langle \nu^2 \rangle_q}}, \quad (42)$$

which has been verified by quenched lattice QCD simulations.

We analyze the partition function (40) for $Z_\nu^{\text{eff}}(m)$ given by the finite-volume partition function in Eq. (39). Replacing the sum over ν by an integral, we obtain after integration

$$Z^{\text{eff}}(\theta, m) = \int_{U \in \text{U}(N_f)} DU e^{-\frac{\langle \nu^2 \rangle_q}{2} (\theta - i \text{Tr} \log U)^2 + \frac{1}{2} \Sigma V \text{Tr} (MU + M^\dagger U^{-1})}. \quad (43)$$

The exponent in the integrand corresponds to the effective static potential of QCD with a large number of colors [38], and therefore the chRMT partition function reproduces all identities that have been derived from this effective potential [20, 39]. For example, the topological charge is screened by light quarks. For a careful analysis of the periodicity requirements of the θ -dependence of the effective partition function (43), see Ref. [40].

Let us illustrate the screening of topological charge for $N_f = 1$ and real m , for which

$$Z^{\text{eff}}(\theta, m) = \int d\phi e^{-\frac{\langle \nu^2 \rangle_q}{2} (\theta - \phi)^2 + \Sigma V m \cos \phi}. \quad (44)$$

The integral over ϕ can be performed by a saddle-point approximation resulting in [23]

$$Z^{\text{eff}}(\theta, m) = e^{mV\Sigma \cos \theta}. \quad (45)$$

The topological susceptibility is given by

$$\langle \nu^2 \rangle = -\frac{\partial^2}{\partial \theta^2} \log Z = mV\Sigma \quad (\text{for } \theta = 0) \quad (46)$$

so that the topological charge is completely screened in the chiral limit. This also shows that the results are insensitive to our choice of the distribution function $P(\nu)$. For example, in an instanton liquid interpretation of the chiral random matrix model, the natural choice for $P(\nu)$ is the binomial distribution $B(N-\nu, \nu)$, resulting in the same effective potential [20].

In fact, it can be concluded from Eq. (46) that for light quarks the distribution $P(\nu)$ can be ignored altogether. Let us again illustrate this for $N_f = 1$, for which the integral in Eq. (39) results in the finite volume partition function

$$Z_\nu^{\text{eff}}(m) = I_\nu(mV\Sigma), \quad (47)$$

where I_ν is a modified Bessel function. Summing over ν according to Eq. (11), i.e. without the weight factors $P(\nu)$, we obtain [41]

$$Z^{\text{eff}}(\theta, m) = \sum_\nu e^{i\nu\theta} I_\nu(mV\Sigma) = e^{mV\Sigma \cos \theta}, \quad (48)$$

where we have used a summation formula for modified Bessel functions. This is exactly the same result as in Eq. (45). For an extension of these results to more than one flavor, see Ref. [41].

3.4 Spectral Correlation Functions

In this section, we discuss the spectral correlation functions and the microscopic spectral density corresponding to the chRMT partition function. The global spectral density is a semicircle. It is not universal and we do not expect to find it in realistic physical systems. The universal quantities are local or microscopic spectral correlation functions. In general, a k -point spectral correlation function is defined by [27]

$$R_k(\lambda_1, \dots, \lambda_k) = \left\langle \sum_{\substack{j_1 \cdots j_k = 1 \\ j_p \neq j_q}}^N \delta(\lambda_1 - E_{j_1}) \cdots \delta(\lambda_k - E_{j_k}) \right\rangle, \quad (49)$$

where the E_{j_p} are eigenvalues. The quantity R_k represents the probability density to find k eigenvalues, regardless of labeling, at $\lambda_1, \dots, \lambda_k$. In particular, $R_1(\lambda) = \rho(\lambda)$. By ‘‘local’’ we mean that the energy differences $|\lambda_p - \lambda_q|$ are of the order of a few mean level spacings.

Because of the $U_A(1)$ symmetry of QCD, all nonzero eigenvalues come in pairs $\pm i\lambda_n$ (see Sec. 2.2.1). This implies that the origin, $\lambda = 0$, is a special point of the spectrum and that we have to consider the R_k separately in the bulk of the spectrum and near $\lambda = 0$. The latter is called the microscopic region or the

“hard edge” of the spectrum.² In addition, there is the tail or “soft edge” of the spectrum, which we do not discuss. The bulk of the spectrum is the middle region, far from either edge.

Because the random matrix partition function is known in terms of an integral over the eigenvalues of the Dirac operator, see Eq. (34), it is possible to obtain the spectral density and all spectral k -point correlation functions by integration over $N - k$ eigenvalues. In the present case, the integrals can be performed most conveniently by the orthogonal polynomial method. We mention only the most important results in the sections below.

3.4.1 BULK CORRELATIONS

Our conventions are such that if we have N eigenvalues, the global spectral density is normalized to N so that the mean level spacing is of order $1/N$. Local spectral correlation functions $R_k(\lambda_1, \dots, \lambda_k)$ in the bulk of the spectrum are thus characterized by $\lambda_p \sim \mathcal{O}(1)$ and $|\lambda_p - \lambda_q| \sim \mathcal{O}(1/N)$. Universal correlation functions are obtained by rescaling the eigenvalues according to the average local level spacing. This procedure, known as unfolding, is discussed in more detail in Sec. 5.1. The rescaled eigenvalues with average level spacing equal to unity are denoted by x_k .

In the bulk of the spectrum, the RMT results for the R_k are identical for the chiral ensembles and the corresponding nonchiral ensembles [42, 43]. For simplicity, let us consider the simplest ensemble, the chUE. On the unfolded scale, we obtain in the limit $N \rightarrow \infty$

$$R_k(x_1, \dots, x_k) = \det[K(x_p, x_q)]_{p,q=1,\dots,k} \quad (50)$$

with the sine kernel

$$K(x, y) = \frac{\sin \pi(x - y)}{\pi(x - y)}. \quad (51)$$

The fact that $K(x, y)$ depends only on $|x - y|$ reflects the translational invariance of the spectral properties after unfolding. The results for the chOE and the chSE are somewhat more complicated than those for the chUE [17].

Other quantities can be derived from the R_k . As a measure of short-range correlations between the eigenvalues, one considers the nearest-neighbor spacing distribution $P(s)$, which is the probability density to have a spacing of s between adjacent levels. In random matrix theories, one finds that $P(s) \sim s^\beta$ for small values of s and has a Gaussian tail for large spacings. Long-range spectral correlations are characterized by the level-number variance $\Sigma^2(L)$ given by

$$\Sigma^2(L) = \langle (n(L) - L)^2 \rangle, \quad (52)$$

where $n(L)$ is the number of levels in an interval of length L , or by the spectral rigidity $\Delta_3(L)$ [44], which is defined as an integral transform of $\Sigma^2(L)$,

$$\Delta_3(L) = \frac{2}{L^4} \int_0^L du (L - u)(L^2 - Lu - u^2)\Sigma^2(u). \quad (53)$$

²The reason for this nomenclature is that in a Fermi-gas formulation of RMT, where the eigenvalues are interpreted as the positions of particles, this symmetry corresponds to choosing a potential that is infinite for negative values of the eigenvalues. In this picture, the soft edge corresponds to a potential with a finite slope.

The advantage of using the Δ_3 -statistic is that its statistical fluctuations are much smaller than those of the Σ^2 -statistic. The quantities Σ^2 and Δ_3 can be derived from the two-point function R_2 . To compute $P(s)$, one needs all k -point functions. These quantities are very different for systems with correlated eigenvalues (described by RMT) and systems with uncorrelated eigenvalues (described by the Poisson ensemble). For example, the large- L behavior of the chUE results is given by $\Sigma^2(L) \sim (\ln L)/\pi^2$ and $\Delta_3(L) \sim (\ln L)/2\pi^2$, whereas for uncorrelated eigenvalues one finds $\Sigma^2(L) = L$ and $\Delta_3(L) = L/15$.

3.4.2 MICROSCOPIC CORRELATIONS

In the context of QCD, the small eigenvalues are more interesting than those in the bulk because of their relation to spontaneous chiral symmetry breaking via the Banks-Casher relation. The local spectral correlation functions at the hard edge of the spectrum are characterized by $\lambda_p \sim \mathcal{O}(1/N)$ and $|\lambda_p - \lambda_q| \sim \mathcal{O}(1/N)$. Unfolding in the microscopic region is easy; the eigenvalues are simply rescaled by the mean level spacing at $\lambda = 0$, which is given by Eq. (23). By convention, we define the unfolded variables by $x_p = \lambda_p V \Sigma$, i.e. the factor of π is omitted. Note that $V \propto N$. Thus, in the unfolded variables we have $x_p \sim \mathcal{O}(1)$ and $|x_p - x_q| \sim \mathcal{O}(1)$. As advertised above, the functional form of the R_k is different in the microscopic region. The R_k are still given by the determinant of a kernel according to Eq. (50), but the sine kernel is now replaced by the Bessel kernel [45],

$$K(x, y) = \sqrt{xy} \frac{x J_{\alpha+1}(x) J_{\alpha}(y) - y J_{\alpha}(x) J_{\alpha+1}(y)}{x^2 - y^2}, \quad (54)$$

where J_{α} denotes Bessel functions and $\alpha = N_f + |\nu|$, with N_f the number of massless flavors and ν the topological charge. A mathematical discussion of the Bessel kernel can be found in Ref. [46].

The RMT results for the chOE and the chSE are more complicated [47, 48, 49, 33]. Note that, in contrast to the situation in the bulk, the microscopic correlations depend on N_f and ν .

The one-point function is universal in the microscopic region. For the chUE, the microscopic spectral density, defined above in Eq. (25), is related to the kernel by $\rho_s(z) = K(z, z)$ and can be expressed as [45, 50]

$$\rho_s(z) = \frac{z}{2} \left[J_{N_f+|\nu|}^2(z) - J_{N_f+|\nu|+1}(z) J_{N_f+|\nu|-1}(z) \right]. \quad (55)$$

It is also the generating function for the Leutwyler-Smilga sum rules, which are essentially inverse moments of ρ_s (or of higher-order spectral correlation functions). They are discussed below. The results (54) and (55) were first derived using chiral RMT. In the meantime, Eq. (55) has been confirmed by an explicit calculation starting from a partially quenched chiral Lagrangian [51, 52], which is discussed in the next section. The microscopic spectral density and the two-point correlation function for the case $N_f + |\nu| = 0$ have also been derived by means of the supersymmetric method of RMT [53].

There is a very interesting connection between the Bessel kernel and the effective partition function. In addition to the partition function $Z^{(N_f)}$ for N_f massless sea quarks, one can also compute the partition function $Z^{(N_f+2)}$ for N_f massless quarks and two additional flavors with imaginary masses. One then

finds the relation [54]

$$K(x, y) = \frac{1}{2}(xy)^{N_f+1/2} \frac{Z^{(N_f+2)}(ix, iy)}{Z^{(N_f)}}, \quad (56)$$

which can also be generalized to massive sea quarks. Thus, to obtain the R_k for N_f flavors, one needs to know the partition function for two additional flavors with imaginary masses. This result has a natural interpretation in terms of the effective spectral partition function (discussed below in Sec. 4). The two additional flavors are the spectral quark and its bosonic superpartner [51]. The relation (56) once again demonstrates the equivalence of the random matrix formulation and the effective field theory in the zero mode domain. Additional consistency conditions for the finite volume partition function are discussed in Ref. [55].

3.5 Universality Proofs

In most random matrix calculations, the probability distribution of the random matrix elements is assumed to be Gaussian to simplify the calculation. Nonuniversal features such as the global spectral density depend on the choice of the probability distribution. On the other hand, universal results of RMT do not depend on this choice, nor on other deformations of the random matrix model. In addition to numerous empirical verifications of universal behavior in RMT, analytical proofs of universality have recently been constructed for two different types of deformations.

First, consider deformations that do not break the invariance of the theory under unitary transformations of the random matrix. In this case, the Gaussian distribution $P(W) \propto \exp(-Na_1 \text{Tr} WW^\dagger)$ is replaced by the more general distribution $P(W) \propto \exp(-N \sum_{k=1}^{\infty} a_k \text{Tr} (WW^\dagger)^k)$, i.e. the quadratic term in the exponent is replaced by an arbitrary polynomial. The advantage of the unitary invariance is that the probability distribution depends only on the eigenvalues of WW^\dagger . For the chiral ensembles, it has been shown that both the bulk and the microscopic spectral correlations remain unchanged on the unfolded scale [49, 56, 57, 58, 59, 60]. The weight function of QCD also contains the fermion determinant, and it has been shown that the universal results are unchanged if the random Dirac matrix in the determinant is replaced by a polynomial of that matrix [61]. Universal microscopic correlations have also been found for the so-called Ginsparg-Wilson Dirac operator [62]. Along with work on universality for the much more widely studied Wigner-Dyson ensembles [63, 64, 65, 66, 67, 68, 69, 57, 70, 71, 72, 73], these findings make it clear that spectral correlations on the scale of the average level spacing are strongly universal, i.e. they do not change despite substantial variations of the average spectral density. There have also been several interesting results on the validity of universality for wide correlators, i.e. on macroscopic scales [64, 65, 66, 74].

Second, consider deformations that do break the unitary invariance by adding an arbitrary deterministic matrix Y to the random matrix W in the Dirac operator. As we discuss in Sec. 6, such a model can provide a schematic description of QCD at nonzero temperature. In particular, the matrix Y can be chosen in such a way that $\rho(0)/V$ vanishes so that chiral symmetry is restored. It has been proven that the bulk correlations on the unfolded scale are unaffected by the

matrix Y , and that the same is true for the microscopic spectral correlations as long as $\rho(0)/V$ remains nonzero [75, 76, 77, 78, 79, 80].

Most universality proofs have been performed for random matrix ensembles with $\beta = 2$. However, it is possible to establish relations between the $\beta = 2$ kernel and the kernels of the other two ensembles with $\beta = 1$ and $\beta = 4$ [47, 81, 82, 83, 84]. From these relations and the universality of the $\beta = 2$ results, one can then infer the universality of the $\beta = 1$ and $\beta = 4$ results. Recently, interesting connections between massive correlators and the massless correlators for $\beta = 1$ and $\beta = 4$ have been made [85], and the transition between these ensembles and the $\beta = 2$ ensemble has been studied [86].

The microscopic spectral correlations are universally given by RMT only if $\rho(0)/V > 0$. An interesting question [87] is what happens to the R_k if there is some phase transition so that $\rho(0)/V$ vanishes. This transition could be triggered by, for example, nonzero temperature or a large number of flavors. Beyond the transition point, there will be a gap in the spectrum, and the smallest eigenvalues beyond this gap are presumably described by the soft-edge results of RMT. What is more interesting, however, is the transition point at which $\rho(0)/V$ becomes zero so that there is no gap. This situation has been investigated in two different ways. First, keeping the unitary invariance, one can fine-tune the polynomial in the exponent of $P(W)$ to make $\rho(0)/V$ just vanish [87]. Second, breaking the unitary invariance, one can choose a “critical” deterministic matrix Y so that $\rho(0)/V = 0$ without a gap [88, 89]. In both cases, one obtains new functional forms for the microscopic spectral correlations and a different scaling with the volume (or matrix dimension). However, the results are not unique; they depend on the way one chooses to approach the $\rho(0)/V = 0$ limit. It is, therefore, an open question as to whether the microscopic spectral correlations of the QCD Dirac operator at the chiral phase transition agree with one of the results obtained in a random matrix model.

4 EFFECTIVE THEORIES AT LOW ENERGIES

4.1 Finite-Volume Partition Function

As we have seen before, chiral symmetry is spontaneously broken by the QCD vacuum. According to Goldstone’s theorem, this leads to the appearance of massless modes. The Lagrangian describing the dynamics of these modes can be obtained solely from the symmetries of the QCD partition function. Goldstone modes corresponding to the symmetry-breaking pattern $SU_R(N_f) \times SU_L(N_f) \rightarrow SU_V(N_f)$ can be parameterized as

$$U = U_R U_L^{-1} \tag{57}$$

with $U_R \in SU_R(N_f)$ and $U_L \in SU_L(N_f)$. The chiral Lagrangian is constructed by the requirement that it should have the same invariance properties as the QCD Lagrangian. In particular, for $m = 0$ the Lagrangian should be both Lorentz invariant and invariant under $SU_R(N_f) \times SU_L(N_f)$. To lowest order in the momenta (or derivatives), the kinetic term in the effective Lagrangian is uniquely given by [6, 7]

$$\mathcal{L}_{\text{kin}} = \frac{F^2}{4} \text{Tr} \partial_\mu U \partial_\mu U^{-1}. \tag{58}$$

The parameter F is the pion decay constant. The mass term in the QCD Lagrangian breaks the full flavor symmetry. However, the full symmetry can be restored if the mass matrix is transformed as well,

$$M \rightarrow U_L M U_R^{-1}. \quad (59)$$

We require that the mass term in the effective Lagrangian satisfies this extended symmetry. To lowest order in M , it is therefore uniquely given by

$$\mathcal{L}_m = -\frac{1}{2} \Sigma \text{Tr} (M U + M^\dagger U^{-1}). \quad (60)$$

For a diagonal mass matrix, the action is therefore minimized by $U = \mathbf{1}$. The normalization of the mass term is such that the mass derivative of the partition function according to Eq. (21) is equal to the chiral condensate Σ . The chiral Lagrangian is valid in the domain

$$m \ll \Lambda \quad \text{and} \quad p \ll \Lambda, \quad (61)$$

where p is the momentum and Λ is a typical hadronic mass scale.

We will study the effective Lagrangian at finite volume in a box of volume L^4 . Then the smallest nonzero-momentum modes are of the order

$$p \sim 1/L. \quad (62)$$

The fluctuations of the zero-momentum modes, the constant fields, are not affected by the kinetic term and are limited only by the mass term. Comparing Eqs. (58) and (60), we see that in a domain where

$$\frac{m \Sigma}{F^2} \ll \frac{1}{L^2}, \quad (63)$$

the fluctuations of the zero-momentum modes completely dominate the fluctuations of the nonzero-momentum modes. The mass-dependence of the effective partition function is then given by [19, 23]

$$Z(m, \theta) = \int_{U \in \text{SU}(N_f)} DU e^{V \Sigma \text{Re Tr } U m e^{i\theta/N_f}}, \quad (64)$$

where we have set $M = m \mathbf{1}$ and have introduced the θ -dependence by the substitution $m \rightarrow m \exp(i\theta/N_f)$ just as for the QCD partition function. Combining the conditions (61) and (63), we find that the finite volume partition function is valid in the domain [19, 23]

$$m \ll \frac{1}{\Lambda L^2} \ll \Lambda. \quad (65)$$

The partition function for a given topological charge can be extracted from its θ -dependence. Since

$$Z(m, \theta) = \sum_{\nu} e^{i\nu\theta} Z_{\nu}(m), \quad (66)$$

we obtain Z_{ν} by Fourier inversion. Thus, the finite volume partition function in the sector of topological charge ν is

$$Z_{\nu}(m) = \frac{1}{2\pi} \int d\theta e^{-i\nu\theta} Z(m, \theta) = \int_{U \in \text{U}(N_f)} DU \det^{\nu} U e^{V \Sigma \text{Re Tr } m U}, \quad (67)$$

which coincides with Eq. (39). The partition function (67) can be evaluated for arbitrary masses. The integrals were first calculated in the context of one-plaquette lattice QCD models [90] but later rederived by means of Itzykson-Zuber integrals [91, 92, 93].

4.2 Leutwyler-Smilga Sum Rules

For masses in the domain of Eq. (65), we can equate the mass dependence of the QCD partition function and the mass dependence of the effective partition function. Equating the coefficients of the expansion in powers of the mass then gives us the so-called Leutwyler-Smilga sum rules [23]. The QCD partition function can be expanded as

$$Z_\nu^{\text{QCD}}(m) = \frac{\langle m^{|\nu|} \prod'_k (m + i\lambda_k) \rangle}{\langle \prod'_k i\lambda_k \rangle} = m^{|\nu|} \left(1 + m^2 \left\langle \sum_{\lambda_k > 0} \frac{1}{\lambda_k^2} \right\rangle + \dots \right), \quad (68)$$

where the prime indicates that the product is over nonzero eigenvalues only. The effective partition function can be expanded in a power series in m as well. From the $U(1)$ part of the group integral, it is clear that $Z_\nu^{\text{eff}}(m) \propto m^{|\nu|}$. Thus,

$$Z_\nu^{\text{eff}} = m^{|\nu|} (a_0 + a_1 m^2 + \dots), \quad (69)$$

where the coefficients a_i are obtained by calculating the group integrals. Let us consider two examples. The simplest example is $N_f = 1$, for which

$$Z_\nu^{\text{eff}} = \frac{1}{2\pi} \int d\theta e^{-i\nu\theta} e^{mV\Sigma \cos\theta} = I_\nu(mV\Sigma). \quad (70)$$

The series expansion of the modified Bessel function is given by

$$I_\nu(x) = \frac{1}{\nu!} \left(\frac{x}{2}\right)^\nu + \frac{1}{(\nu+1)!} \left(\frac{x}{2}\right)^{\nu+2} + \dots \quad (71)$$

for $\nu \geq 0$. We also have $I_{-\nu}(x) = I_\nu(x)$. Matching the normalizations of Eqs. (68) and (69) and equating the coefficients of the $O(m^2)$ terms, we find

$$\left\langle \frac{1}{V^2} \sum_{\lambda_k > 0} \frac{1}{\lambda_k^2} \right\rangle = \frac{\Sigma^2}{4(|\nu| + 1)}. \quad (72)$$

A second example is the case of $\nu = 0$ and arbitrary N_f . In this case, we use the group integral

$$\int DU U_{ij} U_{kl}^\dagger = \frac{1}{N_f} \delta_{jk} \delta_{il} \quad (73)$$

to derive the result

$$\left\langle \frac{1}{V^2} \sum_{\lambda_k > 0} \frac{1}{\lambda_k^2} \right\rangle = \frac{\Sigma^2}{4N_f}. \quad (74)$$

Since asymptotically for large λ the spectral density is proportional to $V\lambda^3$, the sum over the eigenvalues has to be regularized. As discussed above in Sec. 2.3, a finite result is obtained by taking the thermodynamic limit before removing the cutoff.

What do we learn from these sum rules? Since the total number of eigenvalues is of order V , the obvious interpretation is that the smallest eigenvalues are of order $1/V$. Indeed, this is in agreement with the Banks-Casher formula. What is more important, however, is that in the derivation of the sum rules we have relied only on the chiral symmetry of the partition function and its spontaneous breaking by the formation of a chiral condensate. Therefore any theory with

the same pattern of chiral symmetry breaking as QCD should obey the same spectral sum rules. In particular, the eigenvalues distributed according to the chRMT introduced in the previous section should obey the same sum rules. In fact, all Leutwyler-Smilga sum rules can be derived systematically from the joint eigenvalue chRMT probability distribution in Eq. (34) using the known Selberg integrals [94]. In addition to these sum rules, it is possible to derive massive sum rules [95]. A relation between sum rules and partially quenched effective theories was considered in Ref. [96]. Spectral sum rules for Ginsparg-Wilson fermions on the lattice were considered in Ref. [97]. Inverse moments of the small Dirac eigenvalues in generalized chiral perturbation theory were derived in Ref. [98].

We have seen that chRMT allows us to calculate the correlations of the smallest eigenvalues of the Dirac operator on the scale of the average level spacing. This raises the question of whether it is possible to derive the microscopic properties of the eigenvalues from the low-energy effective partition function. The answer is no. The spectral density cannot be derived from the mass dependence of the chiral condensate,

$$\Sigma(m) = \left\langle \frac{1}{V} \sum_k \frac{1}{i\lambda_k + m} \right\rangle, \quad (75)$$

because the average contains the fermion determinant with the same mass. As we show in the next section, this problem can be circumvented by the introduction of a spectral mass.

4.3 Spectral Mass and Partially Quenched Partition Function

The Dirac spectrum can be obtained from the resolvent

$$\Sigma(z) = \left\langle \frac{1}{V} \text{Tr} \frac{1}{\mathcal{D} + z} \right\rangle, \quad (76)$$

where the spectral mass z is an independent complex variable that does not occur in the average. With purely imaginary eigenvalues the spectral density is given by the discontinuity of the resolvent across the imaginary axis,

$$\frac{\rho(\lambda)}{V} = \lim_{\epsilon \rightarrow 0} \frac{1}{2\pi} [\Sigma(i\lambda + \epsilon) - \Sigma(i\lambda - \epsilon)]. \quad (77)$$

This follows immediately upon writing the trace as a sum over the eigenvalues of \mathcal{D} . The generating function for the resolvent can be written down easily [99],

$$Z^{\text{sp}} = \left\langle \frac{\det^{N_f}(\mathcal{D} + m) \det(\mathcal{D} + z)}{\det(\mathcal{D} + z')} \right\rangle_{\text{YM}}, \quad (78)$$

where we have explicitly displayed the fermion determinant in the measure. The resolvent is then given by

$$\Sigma(z) = \frac{1}{V} \partial_z Z^{\text{sp}}(z, z') \Big|_{z'=z}. \quad (79)$$

In QCD, this method was first introduced in order to derive the quenched strong coupling expansion [100]. In nuclear physics and condensed matter physics, this method is known as the supersymmetric method or Efetov method for quenched disorder [101, 102, 103].

The determinants in the numerator can be written as fermionic integrals whereas the determinant in the denominator can be written as a bosonic integral. The partition function (78) is thus invariant under flavor symmetries that mix commuting and anticommuting degrees of freedom. More precisely, for $m = z = z' = 0$ the partition function is invariant under the supergroup $\text{Gl}_R(N_f + 1|1) \times \text{Gl}_L(N_f + 1|1)$. In order to obtain a consistent effective theory, it is essential to extend the unitary symmetry to the general linear group Gl . We expect, as for the QCD vacuum, that chiral symmetry is spontaneously broken to the diagonal subgroup $\text{Gl}_V(N_f + 1|1)$. The mass term explicitly breaks the full symmetry to this subgroup as well.

The effective partition function can be derived in the same way as the regular chiral Lagrangian with one complication. To obtain finite integrals, we must make sure that the integration manifold is Riemannian. This is why we have extended the flavor symmetry to the full general linear group. The integration manifold is then given by the maximum Riemannian submanifold of $\text{Gl}_A(N_f + 1|1)$. In plain language, this means that we compensate the extra minus sign in the supertrace by complexifying the group parameters. The generating function is thus given by [51]

$$Z^{\text{pq}} = \int_{U \in \hat{\text{Gl}}(N_f + 1|1)} DU e^{\int d^4x \left[-\frac{F^2}{4} \text{Str} \partial_\mu U \partial_\mu U^{-1} - \frac{F^2 m_0^2}{12} \left(\frac{\sqrt{2}\Phi_0}{F} - \theta \right)^2 + \frac{\Sigma}{2} \text{Str} (MU + M^\dagger U^{-1}) \right]}, \quad (80)$$

where $i\sqrt{2}\Phi_0/F = \text{Str} \log U$. This partition function is also known as the partially quenched effective partition function. It has been used to obtain a better understanding of quenched lattice QCD results [104, 105]. The hat on Gl denotes the maximum Riemannian submanifold of $\text{Gl}(N_f + 1|1)$, and Str stands for the supertrace. An example of an explicit parameterization of U will be given in the next subsection. The parameter m_0^2 is proportional to the topological susceptibility and results in a mass for the singlet channel that does not vanish in the chiral limit.

The perturbative formulation of this partition function was first given by Bernard and Golterman [104], and a perturbative calculation of the dependence of the condensate on the spectral mass was first performed in Ref. [106]. In that case, it is acceptable to ignore the convergence properties of the effective partition function and integrate over the unitary supergroup instead.

An alternative generating function would be obtained by replacing the ratio of the two determinants by $\det^n(\mathcal{D} + z)$ and putting $n \rightarrow 0$ after having calculated the resolvent. This procedure, known as the replica trick [107], successfully reproduces the asymptotic expansions of the spectral correlation functions [108, 109]. There have been recent claims that it is possible to derive truly nonperturbative results by means of the replica trick [110, 111, 112]. We do not believe that this can be done in general [113, 114, 115]. As mentioned, because of the compact/noncompact structure of the final answer, the supersymmetric formulation is the natural approach to this problem.

4.4 Domains of the Partially Quenched Effective Theory

The Goldstone fields can be written as

$$U = e^{i\sqrt{2}\Pi/F}. \quad (81)$$

To second order in the fields, the effective Lagrangian in momentum space is given by

$$\mathcal{L} = \frac{1}{V} \sum_a \sum_k (k^2 + M_a^2) \Pi_a^2(k), \quad (82)$$

where the sum is over the momenta in a box of length L (including the zero-momentum state) and the masses of the Goldstone bosons are denoted by M_a . The sum over a is over the different Goldstone modes. In addition to the usual Goldstone modes with mass

$$M_{mm}^2 = \frac{2m\Sigma}{F^2}, \quad (83)$$

there are both fermionic and bosonic Goldstone bosons with mass

$$M_{mz}^2 = \frac{(m+z)\Sigma}{F^2} \quad (84)$$

and fermionic and bosonic Goldstone bosons with mass

$$M_{zz}^2 = \frac{2z\Sigma}{F^2}. \quad (85)$$

In the Lagrangian (82), one can distinguish the zero-momentum modes from the nonzero-momentum modes. The magnitude of the fluctuations of the nonzero-momentum modes is of order $1/(k^2 + M_a^2)$, whereas the magnitude of the fluctuations of the zero-momentum modes is of order $1/M_a^2$. Since the smallest nonzero momenta are of order $1/L$, the fluctuations of the zero-momentum modes are dominant if

$$M_a^2 \ll \frac{1}{L^2}. \quad (86)$$

This means that the Compton wavelength of the ‘‘pion’’ is much larger than the size of the box. For nonzero quark masses of order $O(L^0)$, the inequality (86) is never satisfied. However, the spectral mass z is a free parameter, and the inequality can be rewritten as [116, 117]

$$z \ll E_c \equiv \frac{F^2}{\Sigma L^2}. \quad (87)$$

We sometimes refer to the quantity E_c as the Thouless energy for reasons that will become clear in Sec. 7.3. In the domain of Eq. (87), the dominant contributions to the resolvent are from the zero-momentum modes. Thus, the partially quenched effective partition function (80) can be reduced to the partition function in the zero-momentum sector [51, 52],

$$Z = \int_{U \in \hat{\text{Gl}}(N_f+1|1)} DU e^{\frac{1}{2} V \Sigma \text{Str}(MU + M^\dagger U^{-1})}. \quad (88)$$

The microscopic spectral density and the spectral correlations computed from Eq. (88) are identical to those obtained in chRMT [116, 117]. Let us show this by an explicit calculation of the dependence of the chiral condensate on the spectral mass z . To cover the complete range (87), the integral over U has to be done nonperturbatively. This is a straightforward superintegral that can be evaluated using standard methods. The calculation of the integration measure

requires an explicit parameterization of the integration manifold. For example, in the quenched limit, $N_f = 0$, a possible choice is

$$U = \begin{pmatrix} e^{i\phi} & \alpha \\ \beta & e^s \end{pmatrix} \quad (89)$$

with α and β Grassmann variables, $\phi \in [0, 2\pi]$, and $s \in (-\infty, \infty)$. A characteristic feature of the integration manifold is that it consists of a compact and a noncompact component. The valence-quark mass dependence of this partition function and its generalization to arbitrary topological charge coincide with the valence quark mass dependence of the chUE partition function. We merely quote the final result for the resolvent for N_f massless flavors in the sector of topological charge ν [116],

$$\frac{\Sigma(u)}{\Sigma} = u [I_a(u)K_a(u) + I_{a+1}(u)K_{a-1}(u)] + \frac{|\nu|}{u}, \quad (90)$$

where $a = N_f + |\nu|$ and $u = zV\Sigma$. The compact/noncompact symmetries are reflected in the appearance of the I_a/K_a -Bessel functions and are thus a natural ingredient of the underlying integration manifold. This result was first obtained from chRMT by integrating the microscopic spectral density in Eq. (55) as follows,

$$\frac{\Sigma(u)}{\Sigma} = \int_0^\infty d\zeta \frac{2u}{\zeta^2 + u^2} \rho_s(\zeta). \quad (91)$$

Alternatively, the microscopic spectral density can be obtained by taking the discontinuity of $\Sigma(u)$ according to Eq. (77). By integrating back, we find that the mass dependence of the zero-momentum partially quenched partition function coincides with that of the chRMT partition function for $\beta = 2$.

Figure 2 presents a schematic picture of the different domains in the Dirac spectrum. There are other non-QCD theories that can be reduced to the same partially quenched partition function. Probably the best known example is the instanton liquid model of QCD [5]. Another example, more closely related to disordered condensed matter systems, is the random-flux model [118], which is in essence quenched lattice QCD with Kogut-Susskind fermions but without the phase factors due to the γ -matrices. Related examples are so-called two-sublattice models with disorder [119], and disordered lattice models with the chiral and flavor symmetries of QCD [120, 121].

In the range

$$E_c \ll z \ll \Lambda, \quad (92)$$

the effective action (80) is still valid but chiral random matrix theory no longer applies. In this range, the U fields can be expanded to second order in the pion fields, and the spectral mass dependence of the chiral condensate can be obtained to one loop order. The spectral density follows by taking the discontinuity of $\Sigma(z)$ across the imaginary axis. This calculation can be performed both for the partition function of Eq. (80) and the effective partition functions for $\beta = 1$ and $\beta = 4$. The result for the slope of the spectral density at zero, valid for $N_f \geq 2$, reads [122, 26]

$$\frac{\rho'(0)}{\rho(0)} = \frac{(N_f - 2)(N_f + \beta)}{16\pi\beta N_f} \frac{\Sigma}{F^4}. \quad (93)$$

The result for $\beta = 2$ was first derived by Smilga and Stern [122] from the scalar susceptibility in standard chiral perturbation theory. We emphasize that this is

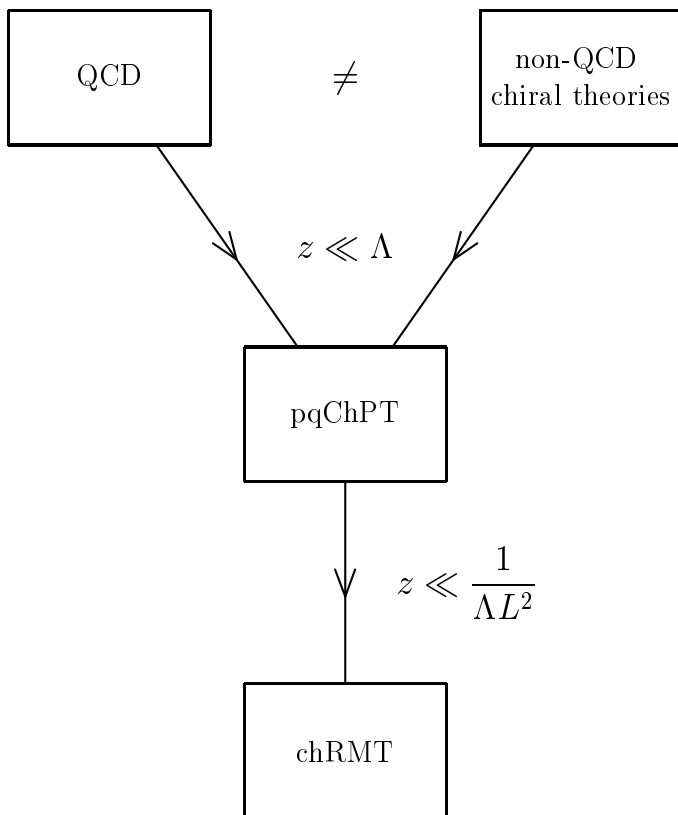


Figure 2: Diagram illustrating the different domains in the QCD Dirac spectrum. Here, pqChPT denotes partially quenched chiral perturbation theory, and chRMT stands for chiral random matrix theory.

an exact result for the QCD Dirac spectrum that is valid in the thermodynamic limit. The vanishing of the slope for $N_f = 2$ has been confirmed by instanton liquid simulations [123].

The two-point correlation function can also be obtained from a supersymmetric generating function with, in this case, two different spectral masses and two bosonic superpartners [51]. Again the zero-momentum contribution coincides with the chUE result. Let us consider the perturbative expansion of the two-point correlation function. Generalizing Eq. (77), we obtain a relation between the two-point level correlation function and the pion susceptibility [51, 124],

$$\langle \rho(\lambda)\rho(\lambda') \rangle^C = \frac{1}{4\pi^2} \frac{\Sigma^2}{F^4} \text{Disc}|_{z=i\lambda, z'=i\lambda'} \sum_q \frac{1}{(q^2 + M^2)^2}, \quad (94)$$

where the meson mass is given by $M^2 = (\sqrt{z^2} + \sqrt{z'^2})\Sigma/F^2$ and the superscript C denotes the connected part of the two-point function. By taking the discontinuities of the zero-momentum contribution, we find the two-point correlation function [51]

$$\langle \rho(\lambda)\rho(\lambda') \rangle^C \sim -\frac{1}{2\pi^2} \left[\frac{1}{(\lambda - \lambda')^2} + \frac{1}{(\lambda + \lambda')^2} \right], \quad (95)$$

which is the correct asymptotic result for the chUE.

4.5 QCD in Three Euclidean Dimensions

QCD in three Euclidean dimensions can be analyzed in much the same way as discussed above. The main difference is the absence of the $U_A(1)$ symmetry and the absence of instantons. In terms of the Dirac spectrum, the eigenvalues do not occur in pairs $\pm i\lambda$, and strictly zero eigenvalues are absent. The Dirac spectrum of this theory on the microscopic scale can be analyzed along the same lines as the four-dimensional theory. The microscopic spectral density and the Leutwyler-Smilga sum rules have been derived [125, 126], the low-energy effective theory has been identified [125, 127], the mass-dependent microscopic spectral density has been found [59, 128], universality has been studied [56, 129], and lattice QCD studies have confirmed the theoretical analysis [130].

5 UNIVERSAL PROPERTIES OF THE LATTICE QCD DIRAC SPECTRUM

5.1 Unfolding

In order to compare eigenvalues of any physical system with RMT results, it is necessary first to “unfold” the empirical spectrum (see e.g. Ref. [131]). The spacing Δ of the eigenvalues is related to the spectral density by

$$\Delta(E) = 1/\rho(E). \quad (96)$$

Unfolding is a local rescaling of the energy scale so that the mean level spacing of the unfolded eigenvalues is equal to unity throughout the spectrum. This is achieved by splitting the spectral density in an average density, $\bar{\rho}(E)$, and a fluctuating piece,

$$\rho(E) = \bar{\rho}(E) + \rho_{\text{fl}}(E). \quad (97)$$

The average spectral density can be obtained in different ways. In some cases, it can be computed analytically using semiclassical arguments. However, in most cases $\bar{\rho}(E)$ is obtained by averaging over many level spacings. There are two essentially different procedures to do this, spectral averaging and ensemble averaging. Spectral averaging is appropriate if only one or a few spectra are available. The average level spacing at E is then obtained by averaging over many level spacings around E . Ensemble averaging is appropriate if there is a large ensemble of spectra all drawn from the same statistical distribution. In this case, the average spacing can be obtained by averaging the spacing at E over each member of the ensemble. In both cases, the separation of the spectral density into an average and a fluctuating piece requires a separation of scales that is typically achieved only in the thermodynamic limit or in the semiclassical limit. The unfolded spectrum, $\{x_n\}$, is then obtained from the average spectral density (equal to the inverse average level spacing) by

$$x_n = \int_{-\infty}^{E_n} \bar{\rho}(\lambda) d\lambda, \quad (98)$$

where $\{E_n\}$ is the original sequence of eigenvalues. The difference between the two procedures is that spectral averaging yields $\bar{\rho}(E)$ separately for each spectrum

whereas ensemble averaging yields a single $\bar{\rho}(E)$ for all spectra. In both cases, the average spectral density of the unfolded spectrum becomes $\bar{\rho}(x) = 1$, so that the sequence $\{x_n\}$ has an average level spacing equal to unity. The correlations of the levels are always calculated for the unfolded spectrum.

The two procedures to calculate the average spectral density do not necessarily give the same spectral correlations at long distances. The equivalence of the two is known as spectral ergodicity. This property has been shown analytically for several random matrix ensembles [132, 133]. In general, ensemble averaging results in stronger level fluctuations than does spectral averaging [134, 135, 136]. In practice a mixture of both methods is often useful. For example, one may calculate the average spectral density by ensemble averaging but, in order to get better statistics, calculate the correlation functions by both ensemble averaging and spectral averaging. Spectral averaging requires that the statistical properties of the eigenvalues be stationary over the spectrum, which is not the case for many systems and has to be checked each time.

5.2 Lattice Tests of Chiral Random Matrix Theory

We have presented a wealth of analytical evidence supporting the statement that the local spectral correlations of the Dirac operator are described by universal functions. Although the Dirac spectrum is not directly observable in experiments, we can compare the predictions of chiral RMT to numerical data obtained by lattice gauge simulations. This is the subject of this section.

This review does not discuss the global spectral density of the QCD Dirac operator. Most lattice results have large finite-size artifacts. Instanton simulations suggest, contrary to random matrix results, that the fermion determinant has a significant effect on the global Dirac spectrum [50, 123, 137, 138].

5.2.1 BRIEF INTRODUCTION TO LATTICE QCD

QCD is a renormalizable quantum field theory that must be regularized. This can be done by formulating the theory on a discrete lattice with lattice spacing a [139]. The largest momentum is then π/a . The quark fields live on the sites and the gauge fields on the links of the lattice. If the lattice is finite, one can simulate the theory on a computer. This can be done efficiently only in Euclidean space, where the gluonic weight function is $\exp(-S_{\text{YM}})$ with S_{YM} real. The discretized form of the Yang-Mills action S_{YM} is the Wilson action S_{W} . The full weight function of QCD also contains the fermion determinants, which can be expressed in terms of the gauge fields. Observables are computed by generating gauge field configurations in a Monte Carlo update procedure and averaging an observable over many configurations. Since the inclusion of the fermion determinants is very time consuming, it is common to use only the gluonic part of the weight function in the Monte Carlo updates. This is called the quenched approximation, which corresponds to the limit $N_f = 0$ or, equivalently, to the limit of infinitely heavy sea quarks. To make contact with continuum physics, the results of lattice simulations must be extrapolated to infinite lattice size (the thermodynamic limit) and to zero lattice spacing (the continuum limit).

Lattice simulations are the main source of nonperturbative information about QCD. Unfortunately, the naive discretization of fermions on a lattice leads to the so-called doubling problem: The quark propagator has poles at each corner of

the Brillouin zone, which gives rise to a total of 2^d species in d dimensions. The unwanted $2^d - 1$ species can be eliminated by adding to the Dirac operator an additional term, the Wilson term, which removes the doublers in the continuum limit. However, this term breaks chiral symmetry explicitly. Another possibility is the use of staggered (or Kogut-Susskind) fermions where one has only one spinor component per lattice site. This maintains a residual chiral symmetry but only partially reduces the number of species to $2^{d/2}$ in the $a \rightarrow 0$ limit. A no-go theorem by Nielsen and Ninomiya [140] states that it is not possible simultaneously to solve the doubling problem and have exact chiral symmetry on the lattice with a local action.

Fortunately, there is a way around this theorem: the remnant chiral symmetry condition of Ginsparg and Wilson [141],

$$\mathcal{D}\gamma_5 + \gamma_5\mathcal{D} = 2a\mathcal{D}\gamma_5 R\mathcal{D}, \quad (99)$$

where R is a spatially local operator that is trivial in Dirac space. In contrast to $\{\mathcal{D}, \gamma_5\} = 0$, chiral symmetry is not exact but is recovered only in the continuum limit $a \rightarrow 0$. Thus, with Dirac operators satisfying Eq. (99), it is possible to get rid of the doublers even at finite lattice spacing without violating the Nielsen-Ninomiya theorem. Recently, several solutions of Eq. (99) have been found in the overlap formalism [142], in the domain-wall formulation in five dimensions [143], and in the perfect action approach [144].

As mentioned in Sec. 2.2.3, there may be cases in which the anti-unitary symmetries of the various lattice discretizations of the Dirac operator differ from those of the continuum operator. In particular, this is true for staggered fermions. In SU(2) color, staggered fermions are in the symmetry class of the chSE, whereas continuum fermions are in the chOE symmetry class. Staggered fermions in the adjoint representation of the gauge group (for any N_c) have the symmetries of the chOE, whereas in the continuum limit the symmetries are those of the chSE. The Wilson Dirac operator \mathcal{D}_W does not anticommute with γ_5 and is therefore not described by any of the chiral ensembles. However, the Hermitian operator $\gamma_5\mathcal{D}_W$ has the same anti-unitary symmetries as the continuum Dirac operator and is described by the corresponding nonchiral ensembles (see also Ref. [145]). Finally, Dirac operators obeying the Ginsparg-Wilson condition, Eq. (99), have the same anti-unitary symmetries as the continuum Dirac operator, but the eigenvalues are located on the complex unit circle [62].

5.2.2 BULK CORRELATIONS

To measure the bulk spectral correlations, one needs all eigenvalues of the Dirac operator, which is represented on the lattice by a finite sparse matrix whose dimension is proportional to the lattice volume and to N_c . The eigenvalues of such a matrix can be obtained using special algorithms, e.g. by the Cullum-Willoughby version of the Lanczos algorithm [146]. On the lattice, this was first done by Kalkreuter [147]. The numerical effort of this method scales with the square of the matrix dimension. For example, in SU(3) on a 10^4 lattice, the Dirac matrix has 15,000 distinct positive eigenvalues, which can be computed on a typical workstation in about 40 minutes. There are exact sum rules for the sum of the squares of all Dirac eigenvalues, which can be used to check the numerical accuracy. Because the number of eigenvalues per configuration is very large and because the ensemble average can be replaced by a spectral average

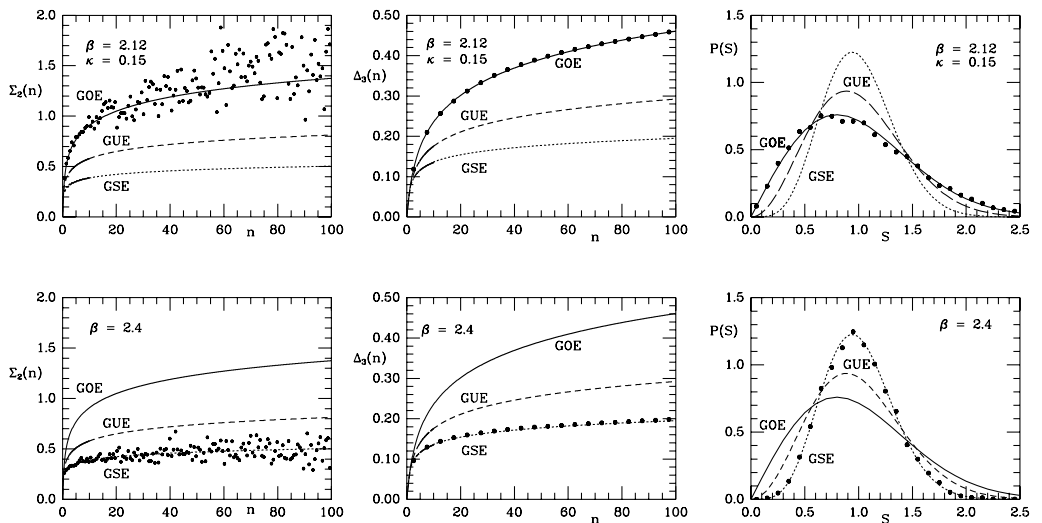


Figure 3: Number variance $\Sigma^2(n)$, spectral rigidity $\Delta_3(n)$, and nearest-neighbor spacing distribution $P(s)$ of the lattice Dirac operator with gauge group $SU(2)$. *Top*: Wilson fermions, $V = 8^3 \times 12$, $N_f = 2$. *Bottom*: staggered fermions, $V = 12^4$, $N_f = 4$, $ma = 0.05$. (From Ref. [149]. Note that in Ref. [149], the figure of $P(s)$ for Wilson fermions shows data points for staggered fermions. This has been corrected in the present figure.)

under the assumption of spectral ergodicity and stationarity, one needs only a few configurations to construct the bulk spectral correlations with great accuracy.

The bulk correlations have been measured in a number of lattice studies for all three symmetry classes [148, 149, 150, 135, 151, 152] and in instanton liquid simulations [137] for $\beta = 2$. As mentioned above, they are insensitive to the number of flavors and the topological charge. In all cases, excellent agreement with the predictions of the appropriate random matrix ensemble was obtained (see e.g. Fig. 3). The agreement is perfect not only in the strong-coupling regime but also at weak coupling. In fact, the bulk spectral correlations are given by RMT even in the deconfinement phase [150, 151], indicating that the gauge fields retain a sufficient degree of randomness in this region of the phase diagram.

Spectral ergodicity was investigated in Ref. [135], and the equivalent of a Thouless energy was found for ensemble averaging, whereas spectral averaging resulted in complete agreement with RMT correlations over distances as long as several hundred average level spacings.

5.2.3 MICROSCOPIC CORRELATIONS

Because only the lowest eigenvalues contribute to the microscopic spectral correlations, a large number of statistically independent spectra are necessary. In contrast to the bulk correlations, the microscopic correlations are sensitive to the number of flavors and the topological charge.

The RMT predictions do not contain an energy scale. In order to make comparisons with lattice data, one needs to determine the energy scale $1/V\Sigma$ to be used in the RMT expressions, see e.g. Eq. (25). This can be done by extracting

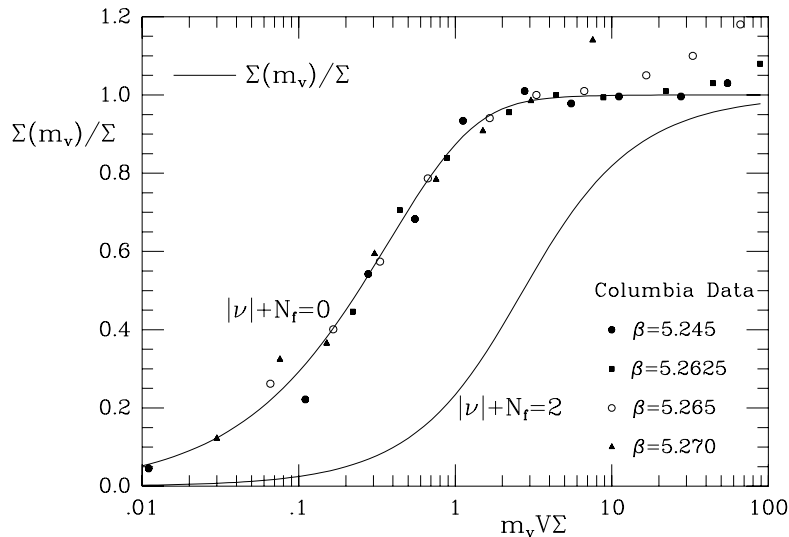


Figure 4: Valence quark mass dependence of the chiral condensate $\Sigma(m_v)$ plotted as $\Sigma(m_v)/\Sigma$ versus $m_v V \Sigma$. The dots and squares represent lattice results by the Columbia group [153] for the values of β indicated in the figure. The solid lines are chRMT results. (From Ref. [116].)

$\rho(0)$ from the data and applying the Banks-Casher relation, Eq. (20). Because this procedure makes no reference to RMT, the comparisons of lattice data with RMT are parameter-free.

The first numerical results for the microscopic spectral density ρ_s were obtained using instanton liquid configurations for $N_c = 2, 3$ and $N_f = 0, 1, 2$ [50], and the expected agreement with the corresponding random matrix predictions was found. The microscopic spectral density was first observed on the lattice via the dependence of the chiral condensate on a valence quark mass m_v , as studied by the Columbia group [153]. Figure 4 shows $\Sigma(m_v)/\Sigma$ as a function of $m_v V \Sigma$ for different values of the coupling constant [116]. The data for different coupling strengths in the broken phase fall on a single curve and agree with the chRMT result for $\Sigma(m_v)$ for $N_f = |\nu| = 0$, see Eq. (90). This figure also shows a deviation from the chRMT predictions at a scale that is of the order of the Thouless energy given in Eq. (87). The spectral mass dependence of the chiral condensate has recently been studied for different symmetry classes and different types of fermions, and a similar quality of agreement has been found [154, 30].

The microscopic spectral correlations have also been investigated in great detail on the lattice [155, 156, 130, 157, 158, 159, 154], and the random matrix predictions were confirmed with very high accuracy for all three symmetry classes. A typical example is shown in Fig. 5.

Although most of these simulations have been performed in the quenched approximation, it is also possible to include dynamical fermions. Deviations from the $N_f = 0$ results are observed only if the sea quarks are very light, with masses on the scale $1/V\Sigma$. Otherwise, the mass term in Eq. (1) dominates the small eigenvalues in the factors of $(i\lambda_n + m_f)$. Analytical results for the microscopic spectral correlations in the presence of sea quarks with mass $\sim 1/V\Sigma$ were obtained in Refs. [160, 161, 162, 163, 85]. Lattice results in this regime agree very

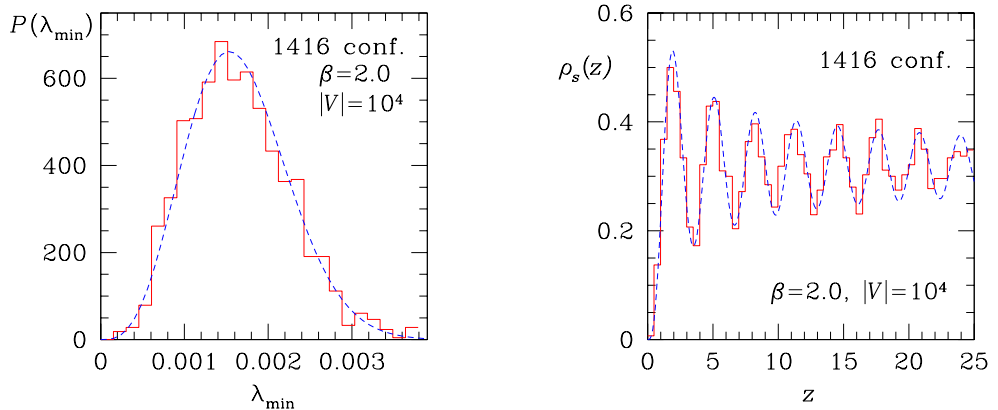


Figure 5: Distribution of the smallest eigenvalue (*left*) and microscopic spectral density (*right*) of the staggered Dirac operator in quenched SU(2). The dashed lines are the predictions of the chSE for $N_f = 0$ and $\nu = 0$. (From Ref. [155].)

well with the corresponding RMT predictions [164]. In the Schwinger model, it is numerically feasible to consider massless sea quarks, and the lattice data are again well described by RMT [165].

Recall that the energy scale for the small eigenvalues is $1/V\Sigma$. Given the agreement of the microscopic spectral quantities with RMT, this means that RMT can be used to determine the infinite-volume chiral condensate Σ [166]. This is most easily done by fitting the numerically determined distribution of the smallest eigenvalue to the RMT result. Since the lattice volume is known, this immediately yields Σ .

5.2.4 TOPOLOGY

The random matrix predictions for the microscopic spectral correlations depend on the number of zero modes of the Dirac operator and, thus, on the topological charge ν of the gauge field configurations. Thus, one should sort the configurations according to their values of ν and make the comparison with RMT separately in sectors of fixed topological charge.

The results presented in the previous section were obtained for the staggered Dirac operator. If one is interested in topological properties, this operator has problems. The zero modes that one would obtain in the continuum limit are shifted at finite lattice spacing a by an amount proportional to a^2 [167]. For reasonable simulation parameters, this amount is larger than the level spacing near zero so that the would-be zero modes are completely mixed with the nonzero modes. Thus, one should expect all spectra of the staggered Dirac operator, even if computed from gauge field configurations with nonzero topological charge, to be described by the RMT results for $\nu = 0$. This was indeed observed in the early data [116, 155] and more recently confirmed in a detailed study (though only in strong coupling) [168]. As the continuum limit is approached, the would-be zero modes should move toward $\lambda = 0$ and eventually separate completely from the nonzero modes. This effect has recently been observed in the Schwinger model in two dimensions [169].

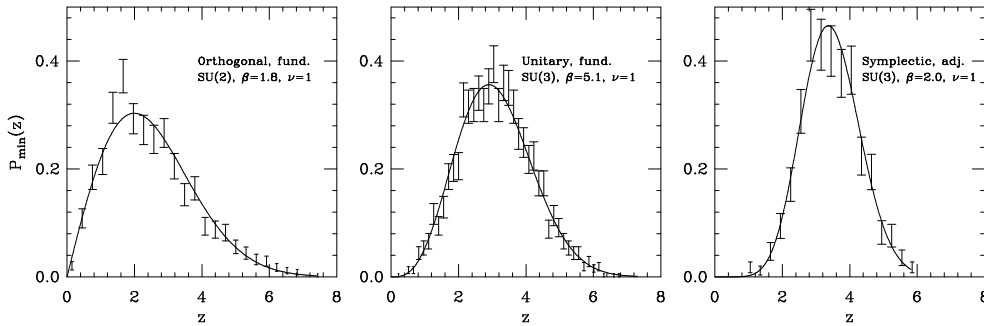


Figure 6: Distribution of the smallest Dirac eigenvalue in the $\nu = 1$ sector for all three symmetry classes. The data were obtained using the overlap Dirac operator on a 4^4 lattice. Solid lines represent the corresponding RMT results. (From Ref. [152].)

Fortunately, Dirac operators satisfying the Ginsparg-Wilson condition (99) do not have this problem. The overlap operator [142] has exact zero modes even at finite lattice spacing, and the microscopic spectral correlations in sectors of fixed ν are in perfect agreement with the corresponding random matrix predictions [165, 152, 154, 30, 170]. Figure 6 shows an example.

5.2.5 CHIRAL PHASE TRANSITION

As mentioned in Sec. 3.5, the microscopic correlations are given by chiral RMT only if $\rho(0)/V > 0$, i.e. if chiral symmetry is spontaneously broken. Chiral symmetry is restored above a critical temperature T_c . The way in which $\rho(0)/V$ approaches zero determines the order of the chiral phase transition and, if it is second-order, the associated critical exponents. Lattice investigations of these questions are very difficult because at finite volume there are no sharp phase transitions. Simulations are plagued by finite-size effects, critical slowing down, and other problems. It is therefore of great interest to investigate the fate of the small Dirac eigenvalues at $T = T_c$ analytically in random matrix models, as was discussed at the end of Sec. 3.5. There are two recent lattice studies of this question [171, 172]. Some of the theoretical expectations were confirmed qualitatively, e.g. the gap in the eigenvalue distribution above T_c and the agreement of the eigenvalue distribution in this region with the soft-edge predictions of RMT. However, further studies are needed to clarify the situation at $T = T_c$. We are looking forward to upcoming work in this area.

5.3 The Thouless Energy and Beyond

As discussed above, the Dirac spectrum is described by chRMT — or, equivalently, by the zero-mode approximation of the low-energy effective theory, — only below the so-called Thouless energy E_c . The theoretical prediction for this quantity [116, 117],

$$E_c \sim \frac{F^2}{\Sigma\sqrt{V}}, \quad (100)$$

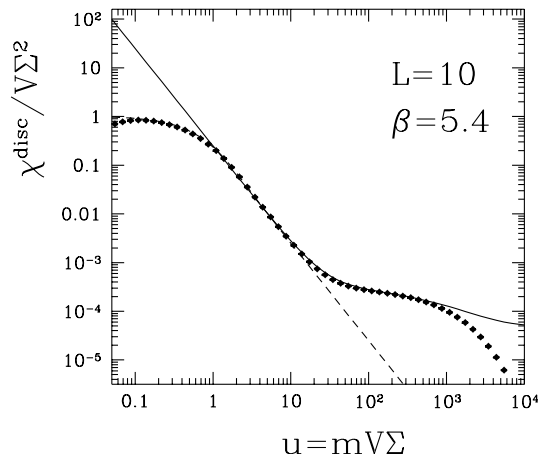


Figure 7: The data points represent the disconnected susceptibility computed on the lattice in quenched SU(3) with staggered fermions ($V = 10^4$, $\beta = 5.4$). The solid line is the prediction of chPT, the dashed line the prediction of chRMT. (The dashed line is hidden by the data points for $u < 10$.) (From Ref. [175].)

has been confirmed quantitatively in the instanton liquid model [137, 173] and on the lattice [174, 158, 135]. To compute the Dirac spectrum beyond the Thouless energy, the calculation must include the kinetic terms in the low-energy effective theory, as discussed in Sec. 4. The results of such an analysis can again be tested by lattice simulations. This has been done for staggered fermions [175]. Note that in this case, the effective low-energy theory must be modified to take into account the symmetries of staggered fermions at finite lattice spacing. A convenient quantity to test the theory is the disconnected scalar susceptibility, defined by

$$\chi^{\text{disc}}(m) = \frac{1}{N} \left\langle \sum_{k,l=1}^N \frac{1}{(i\lambda_k + m)(i\lambda_l + m)} \right\rangle - \frac{1}{N} \left\langle \sum_{k=1}^N \frac{1}{i\lambda_k + m} \right\rangle^2. \quad (101)$$

This quantity can also be computed in chRMT and in chiral perturbation theory (chPT). The result of chRMT is expected to describe the data up to E_c . The result of chPT should describe the data beyond E_c but is expected to break down on the scale of the smallest eigenvalue, i.e. for $m \sim 1/V\Sigma$. These expectations are confirmed by the lattice analysis (see Fig. 7 for an example).

6 SCHEMATIC MODELS

We wish to emphasize again that there are two different types of applications of RMT to physical problems. RMT may be applied as an exact theory for correlations of eigenvalues, as discussed in the first part of this review, or it may serve as a schematic model for chaos and disorder in physical systems. Below, we introduce a random matrix model for the chiral phase transition at nonzero chemical potential and temperature. Random matrix theories as schematic models are mostly used for a description of nonuniversal phenomena. This does not exclude that they describe universal fluctuations of the eigenvalues as well. Typically,

a random matrix model describes both universal and nonuniversal properties. Well-known examples are the Anderson model for localization phenomena [176] and the use of random matrix theory in quantum gravity [177, 178].

We argued in Sec. 1.1 that chiral symmetry breaking can be understood in terms of the stiffness of the Dirac spectrum resulting from interactions of the strong color force. Because spectral stiffness is a characteristic feature of RMT, it is natural to describe the chiral phase transition in terms of a random matrix model. Several different types of schematic random matrix models have been introduced. Here we discuss models for the chiral phase transition at nonzero temperature T , for the chiral phase transition at nonzero chemical potential μ , and for the phase diagram of QCD. We also discuss random matrix models for different types of fermions at $\mu > 0$.

6.1 Chiral Random Matrix Models for the Chiral Phase Transition at Nonzero Temperature

The original motivation for introducing chiral random matrix models was to obtain a better understanding of the QCD Dirac spectrum for temperatures around the critical temperature for the chiral phase transition [179, 180]. The idea is to split the Dirac operator into the time derivative and a remainder that will be replaced by a chRMT,

$$\mathcal{D} = \gamma_0 \partial_0 + R. \quad (102)$$

In a chiral basis with time dependence given by $\exp[i(2n+1)\pi T\tau]$, where τ is the Euclidean time, the first term in \mathcal{D} is diagonal and is given by a direct sum of Matsubara frequencies $\omega_n = (2n+1)\pi T$. The simplest model for \mathcal{D} is obtained by replacing the diagonal matrix with positive Matsubara frequencies by the identity matrix times an effective Matsubara frequency t , and replacing the diagonal matrix with negative Matsubara frequencies by the opposite effective Matsubara frequency. After a suitable basis change, this model can be written (in the sector of zero topological charge) as [179, 180]

$$Z_{N_f}(m) = \int DW \det^{N_f}(\mathcal{D} + m) e^{-\frac{1}{2}N\Sigma^2 \text{Tr}(W^\dagger W)}, \quad (103)$$

where

$$\mathcal{D} = \begin{pmatrix} 0 & iW + it \\ iW^\dagger + it & 0 \end{pmatrix}. \quad (104)$$

We restrict ourselves to the unitary case ($\beta = 2$) with a complex matrix W of dimension $N/2$. The integral is over the real and imaginary parts of the matrix elements of W . For simplicity, we consider only a Gaussian probability distribution. The normalization is such that the parameter Σ is equal to the magnitude of the chiral condensate at zero temperature,

$$\Sigma = \lim_{m \rightarrow 0} \lim_{N \rightarrow \infty} \frac{1}{NN_f} \partial_m \log Z_{N_f}(m) \Big|_{t=0}. \quad (105)$$

It can be shown that the effect of the fermion determinant on the macroscopic spectral density is subleading in N_f/N , so that $\rho(\lambda)$ can be calculated in the quenched limit. By expanding the resolvent of the Dirac operator, defined by

$$G(z) = \frac{1}{N} \text{Tr} \left\langle \frac{1}{z - \mathcal{D}} \right\rangle, \quad (106)$$

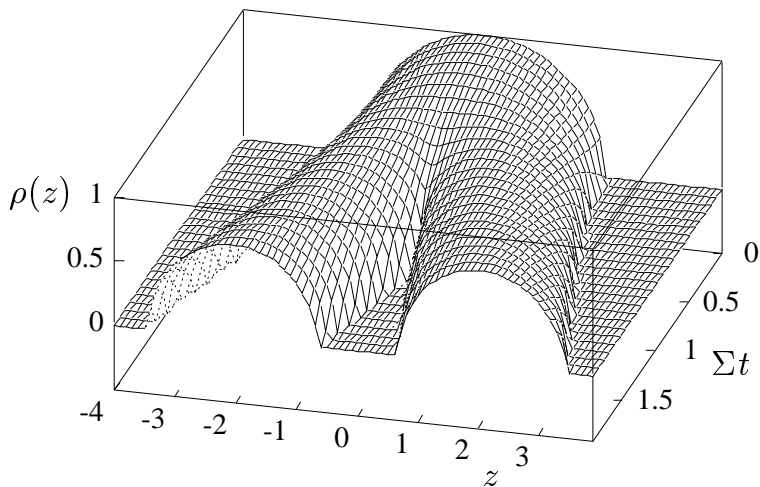


Figure 8: The spectral density of the QCD Dirac operator as a function of an effective Matsubara frequency t that models the effect of temperature. (From Ref. [181].)

in a geometric series of the random matrix, it can be shown that $g = G/\Sigma^2$ satisfies a cubic equation [179, 75, 181],

$$g^3 - 2zg^2 + g(z^2 - t^2 + 1/\Sigma^2) - z/\Sigma^2 = 0. \quad (107)$$

A variant of the method by which this equation was derived in Refs. [179, 75] is sometimes referred to as the Blue's function method [182]. The spectral density, obtained from the discontinuity of the resolvent, is shown in Fig. 8. We observe that chiral symmetry is broken up to $t = 1/\Sigma$ with a chiral condensate given by

$$G(T, z \rightarrow 0) = \Sigma \sqrt{1 - (\Sigma t)^2}. \quad (108)$$

Above this temperature, the spectrum splits into two disconnected regions. Since this model has no spacetime dependence, it should not be a surprise that all critical exponents are given by their mean field values. From Eq. (108), we see that $\beta = 1/2$. For $t \rightarrow 1/\Sigma$, we find

$$G \propto z^{1/3}, \quad (109)$$

resulting in another critical exponent $\delta = 3$. The spectral density at the critical point follows by taking the discontinuity of G across the imaginary axis, see Eq. (77), and is thus given by

$$\rho(\lambda) = \frac{N}{\pi} \lambda^{1/3}. \quad (110)$$

The unfolded eigenvalues in this case are given by

$$x_k = \frac{3N}{4\pi} \lambda_k^{4/3}, \quad (111)$$

and a nontrivial scaling limit at $t = 1/\Sigma$ is obtained by introducing the microscopic variable [88, 89]

$$z = \lambda N^{3/4}. \quad (112)$$

Starting from the exact analytical result derived in Ref. [75], it is possible to take the limit $N \rightarrow \infty$ with the scaling relation (112) and to obtain an analytical result for the microscopic spectral density at the critical point [88, 89]. We emphasize that this result is based on mean field critical exponents and is thus not applicable to QCD with nontrivial critical exponents (see also the discussions in Secs. 3.5 and 5.2.5).

As a last application of the partition function (103), we mention the explanation of the observation [153] that the temperature at which chiral symmetry is restored is higher for gauge field configurations with a nonzero Z_3 -phase than for gauge field configurations with zero Z_3 -phase. The explanation in terms of the random matrix model (103) is that the lowest Matsubara frequency for the nonzero Z_3 -phases is shifted to a lower value by the phase of the Polyakov loop, and thus the critical temperature is higher [181].

6.2 Chiral Random Matrix Models at Nonzero Chemical Potential

6.2.1 QCD PARTITION FUNCTION AT NONZERO CHEMICAL POTENTIAL

The QCD partition function at nonzero temperature T and chemical potential μ is given by [183]

$$Z(m, \mu, T) = \text{Tr} e^{-\frac{H_{\text{QCD}} - \mu N}{T}} = \sum_{\alpha} e^{-\frac{E_{\alpha} - \mu N_{\alpha}}{T}}, \quad (113)$$

where H_{QCD} is the Hamiltonian of QCD with eigenvalues E_{α} and N is the quark number operator. At zero temperature, only the states with $E_{\alpha}/N_{\alpha} < \mu$ contribute to the partition function. We thus expect that the partition function is independent of μ below a critical chemical potential μ_c given by the lightest baryon mass per unit quark number. Therefore, for $\mu < \mu_c \approx m_N/3$ (where m_N is the nucleon mass), the baryon density remains zero and the chiral condensate is constant.

The quark chemical potential appears in the Lagrangian in the form $\mu\psi^{\dagger}\psi = \bar{\psi}(\mu\gamma_0)\psi$ and is therefore introduced in the Dirac operator by the substitution

$$\partial_0 \rightarrow \partial_0 + \mu. \quad (114)$$

This substitution destroys the Hermiticity properties of the QCD Dirac operator, and the resulting complex phase of the fermion determinant makes Monte Carlo simulations impossible. Because of the success of the quenched approximation in lattice QCD simulations at $\mu = 0$, it is tempting to ignore the fermion determinant in this case. However, it was shown [184, 185] that the critical chemical potential for quenched simulations is determined by the pion mass rather than the nucleon mass. Obviously, the basic physics of the problem is not visible in the quenched approximation. An analytical understanding of this problem was first obtained by means of a random matrix model for the Dirac operator of QCD at finite density [186].

6.2.2 A RANDOM MATRIX MODEL FOR QCD AT FINITE DENSITY

A random matrix model for QCD at nonzero chemical potential model is obtained by writing the Dirac operator as [186]

$$\mathcal{D}(\mu) = \mu\gamma_0 + \mathcal{R} \quad (115)$$

and replacing \mathcal{R} by a chiral random matrix ensemble. The partition function is thus given by

$$Z_{N_f}(m) = \int DW \det^{N_f}(\mathcal{D} + m) e^{-\frac{1}{2}N\Sigma^2 \text{Tr}(W^\dagger W)} \quad (116)$$

with a Dirac operator given by

$$\mathcal{D} = \begin{pmatrix} 0 & iW + \mu \\ iW^\dagger + \mu & 0 \end{pmatrix}. \quad (117)$$

For QCD with three or more colors (chUE) this Dirac operator has no Hermiticity properties. Therefore, the fermion determinant in Eq. (116) has a complex phase, and the partition function cannot be simulated by Monte Carlo methods.

The partition function with Dirac operator (117) can be rewritten in terms of a σ -model. For $N_f = 1$, the partition function is particularly simple,

$$Z(\mu) = \int d\sigma d\sigma^* [(\sigma + m)(\sigma^* + m) - \mu^2]^n e^{-n|\sigma|^2}, \quad (118)$$

where we have set $\Sigma = 1$ for ease of notation. For $n = N/2 \rightarrow \infty$ the integrals can be evaluated by a saddle-point approximation. In the chiral limit, we find that [186]

$$\bar{\sigma} = \begin{cases} 0 & \text{for } \mu > \mu_c \Rightarrow Z = \mu^{2n} \\ \sqrt{1 + \mu^2} & \text{for } \mu < \mu_c \Rightarrow Z = e^{-n(\mu^2 + 1)} \end{cases} \quad (119)$$

with μ_c given by the point where the two partition functions are equal, i.e. $\mu_c^2 = \exp(-1 - \mu_c^2)$, which is solved by $\mu_c \approx 0.53$. The vacuum properties of this partition function depend on μ for $\mu \leq \mu_c$. The reason for this unphysical result is discussed below in Sec. 6.2.4. As was demonstrated in Ref. [187] for $\beta = 2$, this model does not show diquark condensation. However, a random matrix model that does show diquark condensation was formulated in Ref. [188].

The QCD partition function (116) is a polynomial in m and μ with coefficients that can be obtained analytically [189]. Its properties can be analyzed by means of its zeros in the complex chemical potential plane and the complex mass plane. Figure 9 shows a first-order phase transition at $\mu \approx 0.53$. In the chirally restored phase, the cut on the imaginary m axis is no longer present. The figure also shows the points (stars) where two solutions of the saddle-point equations of the σ -model coincide. Indeed, the cuts end on these branch points.

In lattice QCD at finite density, the zeros of the QCD function in the complex μ plane can be studied by means of the Glasgow method [190]. This method has been analyzed in terms of the above random matrix model [191] with the conclusion that it requires an exponentially large number of gauge field configurations to obtain statistically significant results.

6.2.3 ZERO TEMPERATURE LIMIT

The random matrix model discussed in the previous section has attracted a great deal of interest, and more sophisticated versions of this model have been proposed [192, 189, 193, 194, 191]. One problem of the model (116) is that the chiral condensate is μ -dependent below the critical value of the chemical potential. The correct zero temperature limit, with a chiral condensate that remains constant up to the critical value of the chemical potential, is obtained if all Matsubara

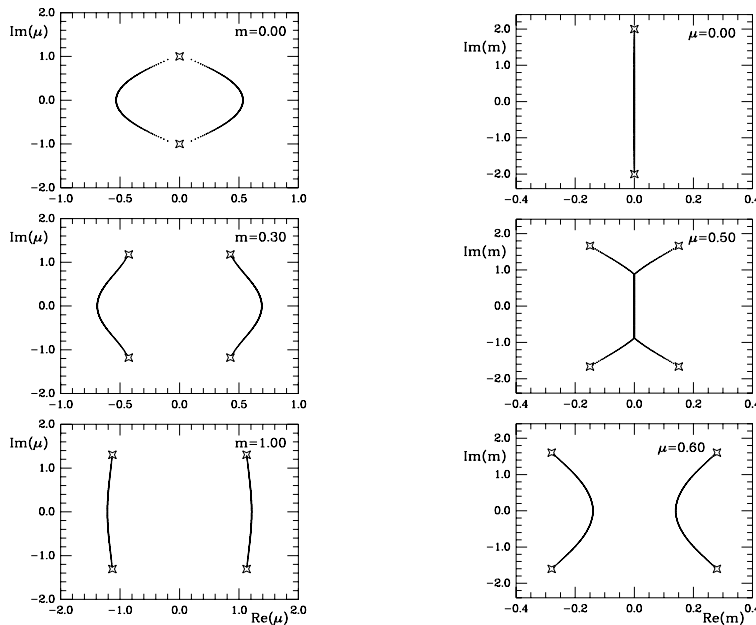


Figure 9: Zeros of the partition function in the complex μ and m plane. (From Ref. [189].)

frequencies are taken into account. We illustrate this with a one-dimensional lattice QCD model.

Writing the Dirac operator as

$$\mathcal{D}(\mu) = \gamma_0(\partial_0 + \mu) + R, \quad (120)$$

the μ -dependence of the fermion determinant can be gauged away by means of a time-dependent gauge transformation, i.e.

$$\gamma_0(\partial_0 + \mu) + R = e^{-\mu\tau} [\gamma_0\partial_0 + R] e^{\mu\tau}. \quad (121)$$

The μ -dependence is now in the boundary conditions, but for $T \rightarrow 0$ we expect that they are not important and that the partition function becomes independent of μ . The lesson is that in order to obtain a condensate that is μ -independent, one must treat the time derivative exactly, or, in other words, all Matsubara frequencies have to be taken into account. This was first worked out in detail for lattice QCD models at nonzero chemical potential [195]. Let us discuss the strong coupling limit of a one-dimensional $SU(N_c)$ lattice QCD model with Kogut-Susskind fermions [196]. In that case, the matrix elements of the discretized Dirac operator are given by

$$\mathcal{D}_{kl} = \delta_{k,l-1} U_{kl} e^\mu - \delta_{k,l+1} U_{kl}^\dagger e^{-\mu}, \quad (122)$$

where the indices are modulo N , the number of lattice sites. Antiperiodic boundary conditions result in an extra minus sign for the matrix elements \mathcal{D}_{1N} and \mathcal{D}_{N1} . The matrices U_{kl} are independent $SU(N_c)$ matrices. By using gauge invariance, one can reduce this partition function to a single $SU(N_c)$ integral, which can be

performed analytically, resulting in the partition function

$$Z_N = 2 \cosh(N_c N \mu) + \frac{\sinh[(N_c + 1)N \sinh^{-1} m]}{\sinh[N \sinh^{-1} m]}. \quad (123)$$

The number of lattice sites N can be interpreted as the total number of Matsubara frequencies. A sharp transition is obtained in the limit $N \rightarrow \infty$. For example, the chiral condensate is given by [196]

$$\lim_{N \rightarrow \infty} \frac{1}{N} \partial_m \log Z_N = \begin{cases} N_c / \sqrt{1 + m^2} & \text{for } \sinh \mu < m, \\ 0 & \text{for } \sinh \mu > m. \end{cases} \quad (124)$$

Similar results have been derived for a large- d strong coupling expansion of lattice QCD at finite density [197] (with d the Euclidean dimensionality). The failure of the quenched approximation has been reproduced in such lattice models. The effect of including all Matsubara frequencies has also been investigated in a random matrix model obtained by replacing the remainder R in Eq. (120) by a chiral random matrix. After ensemble averaging, one obtains a similar partition function with similar conclusions [198].

6.2.4 QUENCHING AT NONZERO CHEMICAL POTENTIAL

The failure of the quenched approximation at nonzero chemical potential was first understood analytically in terms of chRMT by Stephanov [186]. He showed that the quenched limit is the limit $N_f \rightarrow 0$ of a partition function with the absolute value of the fermion determinant,

$$|\det(\mathcal{D}(\mu) + m)|^{N_f}, \quad (125)$$

rather than

$$[\det(\mathcal{D}(\mu) + m)]^{N_f}. \quad (126)$$

The absolute value of the fermion determinant can be written as

$$\det(\mathcal{D} + m) \det(\mathcal{D}^\dagger + m^*) = \det \begin{pmatrix} iW + \mu & m \\ m & iW^\dagger + \mu \end{pmatrix} \det \begin{pmatrix} iW^\dagger - \mu & m^* \\ m^* & iW - \mu \end{pmatrix}. \quad (127)$$

Writing the fermion determinant as a Grassmann integral, we observe that the quenched partition function can be interpreted as a partition function of quarks and conjugate antiquarks. Therefore, in addition to the usual Goldstone modes, we have Goldstone modes consisting of a quark and a conjugate antiquark [199, 186]. Such modes, with the same mass as the usual Goldstone bosons, have a nonzero baryon number. The critical chemical potential given by the mass of the lightest particle with nonzero baryon number is thus $m_\pi/2$. The failure of the quenched approximation thus has an important benefit: It allows us to write down the exact low-energy effective partition function, which is discussed in the next section. The product of the two determinants in Eq. (127) can be written as the determinant of a single Hermitian matrix. This procedure is known as Hermitization [200, 201, 102].

6.2.5 QUENCHED DIRAC SPECTRA

A chRMT for quenched QCD at nonzero chemical potential is obtained by replacing the determinant in Eq. (116) by its absolute value. This model can be

solved analytically in the large- N limit [186]. However, we will follow a different approach by analyzing the corresponding effective theory [202]. The advantage of this approach is that the effective theory is as valid for quenched QCD as it is for the quenched chiral random matrix model.

For non-Hermitian matrices, the eigenvalues are scattered in the complex plane. Using the fact that

$$\partial_{z^*} \frac{1}{z} = \pi \delta^2(z), \quad (128)$$

where the complex delta function is defined as $\delta^2(z) = \delta(\text{Re } z)\delta(\text{Im } z)$, we find that the two-dimensional spectral density is (up to a normalization constant) given by

$$\rho(\lambda) = \frac{1}{\pi} \partial_{z^*} G(z) \Big|_{z=\lambda}. \quad (129)$$

The resolvent is defined as

$$G(z) = \frac{1}{N_f V} \partial_z \log Z, \quad (130)$$

and the quenched result is obtained in the limit $N_f \rightarrow 0$ of the partition function

$$Z = \left\langle \det^{N_f}(\mathcal{D}(\mu) + z) \det^{N_f}(\mathcal{D}^\dagger(\mu) + z^*) \right\rangle. \quad (131)$$

The product in Eq. (131) can be written as

$$\det^{N_f}(\mathcal{D}(\mu) + z) \det^{N_f}(\mathcal{D}^\dagger(\mu) + z^*) = \det \begin{pmatrix} iW \mathbf{1}_{2N_f} + B_R & \zeta \\ \zeta & iW^\dagger \mathbf{1}_{2N_f} + B_L \end{pmatrix} \quad (132)$$

with

$$B \equiv B_R = B_L = \begin{pmatrix} \mu \mathbf{1}_{N_f} & 0 \\ 0 & -\mu \mathbf{1}_{N_f} \end{pmatrix} \quad \text{and} \quad \zeta = \begin{pmatrix} z \mathbf{1}_{N_f} & 0 \\ 0 & z^* \mathbf{1}_{N_f} \end{pmatrix}, \quad (133)$$

where we have displayed the degeneracy in flavor space by means of the identity matrices $\mathbf{1}_{2N_f}$ and $\mathbf{1}_{N_f}$. For $z = \mu = 0$, the quenched partition function is thus invariant under $SU_R(2N_f) \times SU_L(2N_f)$. This symmetry is broken spontaneously to the diagonal subgroup, $SU_V(2N_f)$. At low energies, the effective partition function is therefore given by a partition function of Goldstone modes parameterized by matrices $U \in SU(2N_f)$. The static effective Lagrangian is obtained from the requirement that it should have the same symmetries as the underlying microscopic partition function. The mass term was discussed in Sec. 4.1. The chemical potential term remains invariant under $SU(2N_f) \times SU(2N_f)$ transformations if at the same time B_R and B_L , now considered as independent matrices, are transformed as

$$B_R \rightarrow U_R B_R U_R^{-1}, \quad B_L \rightarrow U_L B_L U_L^{-1}. \quad (134)$$

The matrices U in the Goldstone manifold transform as $U \rightarrow U_R U U_L^{-1}$. To lowest nontrivial order in μ , we can write two invariant combinations,

$$\text{Tr } U B_L U^{-1} B_R \quad \text{and} \quad \text{Tr } B B. \quad (135)$$

The coefficients follow from the conditions that the critical chemical potential is equal to one third of the mass of the lightest baryon and that the baryon density

should vanish below μ_c . For the static limit of the effective partition function, we find

$$Z = \int_{U \in \text{SU}(2N_f)} DU e^{-\frac{F^2 V}{4} \text{Tr}[U, B][U^{-1}, B] + \frac{1}{2} \Sigma V \text{Tr}(MU + M^\dagger U^{-1})}, \quad (136)$$

with the mass matrix given by

$$M = \begin{pmatrix} z \mathbf{1}_{N_f} & 0 \\ 0 & z^* \mathbf{1}_{N_f} \end{pmatrix}. \quad (137)$$

This partition function can be derived more elegantly by means of a local gauge invariance principle [203, 204]. For real masses z the Dirac operator satisfies the relation $\det(\mathcal{D}^\dagger(\mu) + z^*) = \det(\mathcal{D}(-\mu) + z)$, so that the partition function defined in Eq. (131) and the corresponding low-energy effective partition function given in Eq. (136) can be interpreted as the partition function of QCD at finite isospin density [205].

Below the critical chemical potential, $\mu < m_\pi/2$, only the vacuum state contributes to the partition function, so that

$$Z = e^{\Sigma V N_f (z + z^*)}. \quad (138)$$

In terms of the effective theory, the saddle point is at $U = \mathbf{1}$. The resolvent (130) is given by

$$G(z) = \frac{1}{N_f V} \partial_z \log Z = \Sigma. \quad (139)$$

Since $G(z)$ does not depend on z^* , it follows from Eq. (129) that the spectral density is zero in the region where (139) holds. Because $m_\pi^2 = (z + z^*)\Sigma/F^2$, see Eqs. (83) through (85), the condition $\mu < m_\pi/2$ means that the spectral density vanishes everywhere except in a strip

$$|\text{Re } z| < \frac{2\mu^2 F^2}{\Sigma}. \quad (140)$$

For z inside this strip, the Goldstone modes contribute to the partition function. In terms of the effective partition function, the saddle point rotates away from $U = \mathbf{1}$, leading to a nonvanishing diquark condensate. The rotation of the saddle point is a generic feature of low-energy effective partition functions of non-Hermitian field theories [206, 207, 203, 204, 208].

These results are in qualitative agreement with spectra of the quenched lattice QCD Dirac operator at $\mu \neq 0$ [184]. The correlations of the complex eigenvalues are not so well understood, but the first lattice QCD calculations [209] seem to confirm the theoretical expectations [210, 211, 212, 213].

6.3 Phase Diagram for the QCD Partition Function

The random matrix models at nonzero temperature and nonzero chemical potential introduced in the previous sections can be merged into a single schematic chRMT model for the chiral phase transition [183],

$$Z = \int DW \det^{N_f} \begin{pmatrix} m & iW + iC \\ iW^\dagger + iC & im \end{pmatrix} e^{-\frac{1}{2} N \Sigma^2 \text{Tr} WW^\dagger}, \quad (141)$$

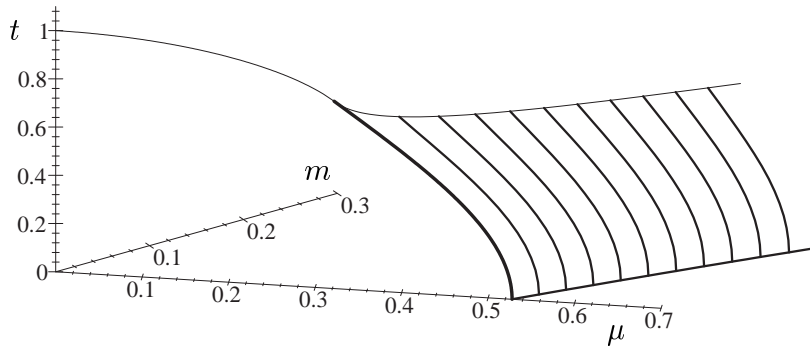


Figure 10: Phase diagram of QCD with two light flavors of mass m as calculated from the random matrix model. The almost parallel curves on the wing surface are cross sections of this surface with $m = \text{constant}$ planes. (From Ref. [183].)

where C is a diagonal matrix with $C_{kk} = t - i\mu$ for one half of the diagonal elements and $C_{kk} = -t - i\mu$ for the other half. In the following, we set $\Sigma = 1$ for simplicity.

This random matrix partition function can be rewritten as a σ -model. For the case $N_f = 1$ it is given by

$$Z(t, \mu) = \int d\sigma e^{-\frac{N}{2} \text{Tr} \Omega(\sigma)}, \quad (142)$$

where

$$\begin{aligned} \Omega(\sigma) = & \sigma\sigma^* - \frac{1}{2} \log[(\sigma + m)(\sigma^* + m) - (\mu + it)^2] \\ & - \frac{1}{2} \log[(\sigma + m)(\sigma^* + m) - (\mu - it)^2]. \end{aligned} \quad (143)$$

For $t = 0$ this is exactly the σ -model discussed in Sec. 6.2.2. At the saddle point, the chiral condensate is given by the expectation value of σ . For $m = 0$ the saddle-point equation is of fifth order in σ ,

$$\sigma[\sigma^4 - 2(\mu^2 - t^2 + \frac{1}{2})\sigma^2 + (\mu^2 + t^2)^2 + \mu^2 - t^2] = 0. \quad (144)$$

The critical points occur where one of the solutions of the quartic equation merges with the solution $\sigma = 0$, i.e. along the curve $(\mu^2 + t^2)^2 + \mu^2 - t^2 = 0$. At the tricritical point, three solutions merge. This happens if in addition $\mu^2 - t^2 + \frac{1}{2} = 0$.

Figure 10 shows the phase diagram in the $\mu t m$ -space. In the $m = 0$ plane, we observe a line of second-order phase transitions and a line of first-order phase transitions. They join at the tricritical point. Also joining at the tricritical point is a line of second-order phase transitions in the m -direction, which is the boundary of the plane of first-order transitions in $\mu t m$ -space. This line is the collection of end points of lines of first-order phase transitions. We expect that the critical exponents for such a liquid-gas transition are given by the three-dimensional Ising model. The tricritical point was also found in a Nambu–Jona-Lasinio model [214, 215].

Because the saddle-point equation (144) is of fifth order in σ , the critical properties of the random matrix model (141) are very similar to those of a ϕ^6 -theory. The critical dimension at the tricritical point of such theories is three, so that mean field theory, and therefore RMT, describes the correct critical behavior at this point. This random matrix model can be considered as the matrix equivalent of a Landau-Ginzburg functional. The advantage over using the standard Landau-Ginzburg theory is that in this case the spectrum of the Dirac operator is also accessible. This allows us to study the critical properties of the Dirac eigenvalues. For example, for $\mu = 0$ we have found that the distribution of the smallest nonzero eigenvalue of the Dirac operator may serve as an order parameter for the chiral transition [179].

6.4 Random Matrix Triality at $\mu \neq 0$

In previous sections, we have shown that the pattern of chiral symmetry breaking and the correlations of the Dirac eigenvalues are related to the anti-unitary symmetries of the Dirac operator. Since the chemical potential occurs only in the combination $\partial_0 + \mu$, the anti-unitary symmetries at $\mu \neq 0$ are the same as for zero chemical potential. Thus for QCD with two colors and fermions in the fundamental representation the Dirac operator is real ($\beta = 1$), whereas for QCD with adjoint fermions the Dirac operator is quaternion real ($\beta = 4$). In the first case, the Dirac operator has the structure [193]

$$\mathcal{D} = \begin{pmatrix} 0 & W + \mu \\ -W^T + \mu & 0 \end{pmatrix} \quad \text{with } W \text{ real.} \quad (145)$$

In the second case, \mathcal{D} is given by

$$\mathcal{D} = \begin{pmatrix} 0 & W + \mu \\ -W^\dagger + \mu & 0 \end{pmatrix} \quad \text{with } W \text{ quaternion real.} \quad (146)$$

In this case, the quaternion real matrix elements of W satisfy the reality relation $W_{kl}^* = \sigma_2 W_{kl} \sigma_2$. In both cases, it is easy to show that the fermion determinant is real. Furthermore, because of

$$\det^{N_f} W \det^{N_f} W^T = \det^{2N_f} W \quad \text{for } \beta = 1, \quad (147)$$

$$\det^{N_f} W \det^{N_f} W^\dagger = \det^{2N_f} W \quad \text{for } \beta = 4, \quad (148)$$

the flavor symmetry group is enhanced to $U(2N_f)$ in both cases (for $\nu = 0$).³ The full flavor symmetry is broken spontaneously to $Sp(2N_f)$ and $O(2N_f)$, respectively, and is broken in the same way by the mass term. The chemical potential breaks the symmetry according to $U(2N_f) \rightarrow U(N_f) \times U(N_f)$ in both cases. For both $\beta = 1$ and $\beta = 4$ the pseudoreality of the Dirac operator leads to Goldstone modes with a nonzero baryon number in the same way we have seen for the phase quenched partition function. An exact low-energy effective partition function valid to lowest order in m and μ^2 can be written down [204].

³For $\beta = 4$ and $\mu = 0$, the Dirac operator satisfies the relation $(C\mathcal{D})^T = -C\mathcal{D}$ whereas $(C\mu\gamma_0)^T = C\mu\gamma_0$ (with C the charge conjugation matrix). Therefore, for $\beta = 4$ and $\mu \neq 0$, the Pfaffian of the Dirac operator is not defined and the fermion determinant $\det^{N_f/2}(\mathcal{D} + \mu\gamma_0)$ cannot be expressed as an integral over N_f Majorana fermions with flavor symmetry $U(N_f)$, as discussed in Sec. 2.2.3. Instead, we write $\det^{N_f}(\mathcal{D} + \mu\gamma_0)$ as an integral over N_f Dirac fermions with flavor symmetry $U(2N_f)$.

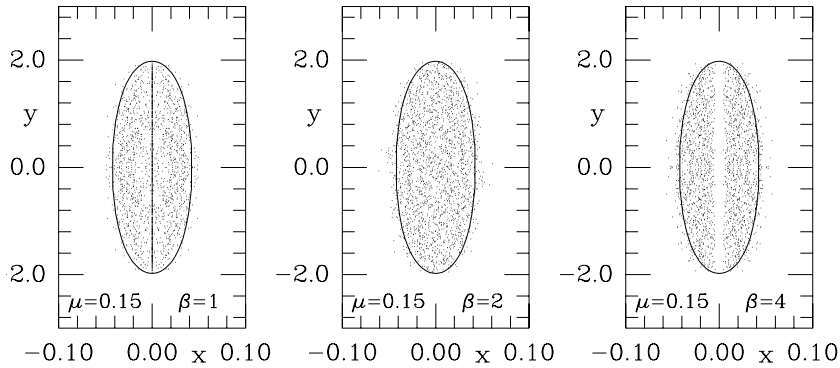


Figure 11: Scatter plot of the real (x) and imaginary (y) parts of the eigenvalues of the random matrix Dirac operator at nonzero chemical potential. The values of β and μ are given in the figures. Full curves show the analytical result for the boundary. The line along the imaginary axis for $\beta = 1$ represents the accumulation of eigenvalues on this axis. (From Ref. [193].)

For an elaborate discussion of the symmetries, their breaking pattern, and the low-energy effective theory in both cases, see Ref. [204].

For an even number of flavors, dynamical Monte Carlo simulations are possible for $\beta = 1$ and $\beta = 4$, though not for $\beta = 2$. However, quenched simulations have been performed for all three classes. A cut along the imaginary axis below a cloud of eigenvalues was found in instanton liquid simulations [216] for $N_c = 2$ at $\mu \neq 0$, which corresponds to $\beta = 1$. In lattice QCD simulations with staggered fermions for $N_c = 2$ [217], a depletion of eigenvalues along the imaginary axis was observed, whereas for $N_c = 3$ the eigenvalue distribution did not show any pronounced features [184].

A chiral random matrix model for the Dirac operator at $\mu \neq 0$ in each symmetry class is obtained by drawing the matrix elements of W from a Gaussian probability distribution. In the quenched approximation, the spectral properties of the random matrix Dirac operator of Eq. (117) can easily be studied numerically by diagonalizing a set of matrices with the probability distribution of Eq. (116). Figure 11 shows results [193] for the eigenvalues of a few 100×100 matrices for $\mu = 0.15$ (dots). The solid curves represent the analytical result for the boundary of the domain of eigenvalues derived in Ref. [186] for $\beta = 2$. However, the analysis can be extended [193] to $\beta = 1$ and $\beta = 4$, and with the proper scale factors, the solution is identical.

For $\beta = 1$ and $\beta = 4$ we observe exactly the same structure as in the previously mentioned (quenched) QCD simulations. There is an accumulation of eigenvalues on the imaginary axis for $\beta = 1$ and a depletion of eigenvalues along this axis for $\beta = 4$. The depletion can be understood as follows. For $\mu = 0$ all eigenvalues are doubly degenerate. This degeneracy is broken at $\mu \neq 0$, which produces the observed repulsion between the eigenvalues.

The number of purely imaginary eigenvalues for $\beta = 1$ scales as \sqrt{N} and is thus not visible in a leading-order saddle-point analysis. Such a \sqrt{N} scaling is typical for the regime of weak non-Hermiticity first identified by Fyodorov et al. [211]. Using the supersymmetric method of RMT, Efetov [207] obtained

the \sqrt{N} dependence analytically. The case $\beta = 4$ was also analyzed analytically [218], with results that are in complete agreement with the numerical simulations. Obviously, more work is needed in order to arrive at a complete characterization of universal features [212] of the spectrum of non-Hermitian operators.

7 RELATED MODELS AND RELATIONS TO OTHER FIELDS

Random matrix theory has been used extensively in many different fields including nuclear physics, atomic and molecular physics, condensed matter physics, quantum chaos, quantum gravity, and mathematical physics. Before reviewing a few applications that might have some relation to QCD, we briefly discuss another class of matrix models for the QCD partition function. For a more comprehensive review of the material in this section, see Refs. [18, 219, 220, 221, 222].

7.1 One-Plaquette Models of Lattice QCD

One class of matrix models for QCD are lattice QCD partition functions on a 2^d lattice. The simplest model in this class is the one-plaquette partition function for pure gauge theory in $d = 2$. This model is known as the Brézin-Gross-Witten model [223] and is defined by

$$Z(J, J^\dagger) = \int_{U \in U(N)} DU e^{\text{Tr}(JU^\dagger + J^\dagger U)}, \quad (149)$$

where the integral is over the Haar measure of $U(N)$ and J is an arbitrary complex source term. We have shown that this partition function can be expressed as a determinant of modified Bessel functions [90, 23, 93]. For J a multiple of the identity (with the interpretation of $J \sim 1/g^2$, where g is the Yang-Mills coupling constant), this model was solved analytically in the large- N limit by Gross and Witten. They found a third-order phase transition at a critical value of J . A large- N chiral phase transition is obtained by extending this model with a fermion determinant [224]. Despite considerable effort, the generalization of this model to more than two dimensions, which is known as the Eguchi-Kawai model [225], could not be solved analytically [226].

The Brézin-Gross-Witten model [223] can be rewritten as a generalized Kontsevich model, which has received a great deal of attention in the theory of exactly integrable systems [227, 222]. There are many other relations between RMT and the theory of exactly solvable systems. Among others, the asymptotic properties of correlation functions can be derived by means of conformal field theory [228]. An interesting overview in the context of string theory is given in Ref. [227].

Another class of related models is the Kazakov-Migdal model [229], which is also known as induced QCD. In its simplest form it is defined by

$$Z = \int DH DU e^{\sum_x \text{Tr} H^2(x) + \sum_{x,\mu} \text{Tr} [U(x)H(x)U^\dagger(x)H(x+\mu)]}, \quad (150)$$

where the $H(x)$ are Hermitian matrices and the $U(x)$ are unitary matrices. The sum is over a lattice in d dimensions. A zero-dimensional form of this model was proposed as a model for the transition between Poisson statistics and Wigner-Dyson statistics [230, 173].

7.2 Universal Conductance Fluctuations in Disordered Mesoscopic Systems

In condensed matter physics, a mesoscopic system is a system whose linear size is larger than the elastic mean free path of the electrons but smaller than the phase coherence length, which is essentially the inelastic mean free path. A typical size is about $1 \mu\text{m}$. The conductance g of mesoscopic samples is closely related to their spectral properties. Using a scaling block picture, Thouless found that in the diffusive regime, the conductance is given by $g = E_C/\Delta$, where E_C/\hbar is the inverse diffusion time of an electron through the sample and Δ is the mean level spacing [231]. This can be rewritten as $g = \langle N(E_C) \rangle$, where $\langle N(E) \rangle$ is the mean level number in an energy interval E . Thus the variance, $\langle \delta g^2 \rangle$, of the conductance is related to the number variance, Σ^2 , of the energy levels [232].

Low-temperature experiments have been performed in which the conductance of mesoscopic wires was measured as a function of an external magnetic field. The observed fluctuations in g are of the order of e^2/h , independent of the details of the system (shape, material, etc). These are the so-called universal conductance fluctuations [233]. One can understand this phenomenon qualitatively by estimating the number fluctuations of the electron levels using RMT results. Both the magnitude of the fluctuations and their universality can be obtained through the transfer matrix method. An interesting numerical result is that the density of eigenvalues of the transmission matrix in the Hofstadter model for universal conductance fluctuations can be described in terms of the microscopic spectral density of the chUE [234, 235].

7.3 Anderson Localization

In more than two dimensions, a good conductor becomes an insulator when the disorder becomes sufficiently strong. This phenomenon is called Anderson localization. In the localized phase, the wave function of the electron is not described by Bloch waves, but by a localized form that decays exponentially,

$$\psi(r) \sim e^{-r/L_c} . \quad (151)$$

The length scale L_c is known as the localization length. This phenomenon was first described by the Anderson model [176], which is a hopping model with a random potential on each lattice point. The dimensionality of the lattice plays an important role. It has been shown that in one dimension all states are localized. The critical dimension is two, whereas in three dimensions there is a delocalization transition at an energy E_L . The states below E_L are localized whereas the states above E_L are extended, i.e. with a wave function that scales with the size of the system. The eigenvalues of the localized states are not correlated, and their correlations are described by the Poisson distribution.

An interesting question is whether Dirac eigenfunctions can be exponentially localized. Parisi argued that localized states can only occur in quenched systems [236]. In QCD this argument goes as follows. If the eigenfunctions were spatially localized, the eigenvalues would be uncorrelated, and there would be no repulsion between the eigenvalues. Because of the fermion determinant and the measure in Eq. (34), the eigenvalues would be repelled from the origin. Since there would be no mechanism to compensate for this repulsion, $\rho(0)/V$ and the chiral condensate would be zero. Therefore, if chiral symmetry is spontaneously broken,

the eigenfunctions of the Dirac operator must be spatially extended. Indeed, this has been found for the wave functions of the Dirac operator for a gauge field ensemble given by a liquid of instantons [137] as well as in lattice QCD [237].

In the extended domain, the situation is more complicated. An important energy scale is the Thouless energy [231], which is related to the diffusion time of an electron through the sample (see Sec. 7.2). With that diffusion time given by L^2/D (the diffusion constant is denoted by D), the Thouless energy is [238]

$$E_c = \frac{\hbar D}{L^2}. \quad (152)$$

On time scales larger than \hbar/E_c , an initially localized wave packet diffuses all over phase space. If this wave function $\psi(t)$ at $t > \hbar/E_c$ is expressed as a superposition of eigenfunctions $\phi_i(t=0)$, many of the overlaps $\langle \psi(t) | \phi_i \rangle$ are nonzero. Therefore we expect that for energy differences below E_c the eigenvalues are correlated according to RMT.

The diffusive behavior of electrons is described by Goldstone modes, called diffusons. Classically, they satisfy a diffusion equation [238, 239, 102]. The diffusion modes can be described in terms of a σ -model, which has the same structure as the low-energy effective theory for the QCD partition function. The Thouless energy corresponds to the energy scale below which the fluctuations of the zero-momentum modes dominate the fluctuations of the nonzero-momentum modes, i.e. the scale discussed in Sec. 4.4, below which the QCD Dirac spectra are given by chRMT. The analysis of classically chaotic quantum systems has made it clear that spectra are described by RMT if and only if the corresponding classical motion is chaotic [240, 241]. If we interpret the Dirac operator as a Hamiltonian in four Euclidean dimensions plus one artificial time dimension, we thus conclude that the classical motion of the quarks is chaotic⁴ [99] and therefore diffusive in four Euclidean dimensions and one artificial time dimension, in agreement with the interpretation of Goldstone modes as diffusion modes [239, 243]. The equivalent of the diffusion constant can be read off immediately by comparing the two σ -models, or equivalently by comparing the scale of Eq. (87) with the Thouless energy, and is given by $D \sim F^2/\Sigma$ [137, 244]. Quantum mechanically, the Thouless energy can be interpreted as the spreading width of the exact eigenstates over the states of the noninteracting Hamiltonian [245, 246].

7.4 Non-Hermitian Models with Disorder

In the past few years, several non-Hermitian models with disorder have been introduced in the literature. We mention only the simplest model, which was motivated by the study of flux-line pinning in superconductors [247, 248]. Its Hamiltonian is given by

$$H = \frac{1}{2m}(\mathbf{p} + i\mathbf{h})^2 + V(\mathbf{r}), \quad (153)$$

where $V(\mathbf{r})$ is a random disorder potential, \mathbf{p} is the momentum operator, and $i\mathbf{h}$ is a constant imaginary vector potential. The new feature of such models is that a localization-delocalization transition can occur even in one and two dimensions. Although the wave functions corresponding to real eigenvalues remain localized,

⁴There is an elaborate literature on the classical dynamics of gauge fields. For a discussion of this topic, see Ref. [242].

the wave functions of complex eigenvalues can be extended. For a detailed discussion of such models, see Refs. [201, 249].

The dependence on \mathbf{h} in the Hamiltonian H occurs only in the combination $\mathbf{p} + i\mathbf{h}$, i.e. in exactly the same way as the chemical potential in the QCD Dirac operator. There are two important differences from QCD: (a) the operator H does not have a chiral structure, and (b) the disorder is uncorrelated Gaussian and quenched. The connection between delocalization in the Hatano-Nelson model (153) and diquark condensation in quenched QCD at nonzero chemical potential is not yet understood and deserves further attention.

After the initial work of Ginibre [210], non-Hermitian RMT has received a great deal of attention in the mathematics literature as well. Probably the best overview of results in this area is in the book by Girko [200].

7.5 Andreev Scattering

The term Andreev scattering (or Andreev reflection) refers to a process in which an electron hits the interface between a normal metal and a superconductor and is reflected as a hole with the opposite momentum (or vice versa) [250]. Stated differently, two electrons can tunnel through the interface so that a Cooper pair is added to the superconducting condensate (or removed from it). This process can be described in a microscopic mean field model by the Bogoliubov-deGennes Hamiltonian, which can be written in matrix form as

$$H = \begin{pmatrix} A & B \\ B^\dagger & -A^T \end{pmatrix}, \quad (154)$$

where A ($-A^T$) represents the Hamiltonian for particles (holes) and B represents the pairing field. The requirement that H be Hermitian means that A must be Hermitian. If the system under consideration is invariant under time reversal or spin rotation or both, there may be additional symmetries. If the system is invariant under spin rotation, B is symmetric (in this case we consider the Hamiltonian in the space of spin-up states only). If, in addition, the system is invariant under time reversal, the elements of H are real. Otherwise, they are complex. On the other hand, if the system is not invariant under spin rotation, B is antisymmetric. In this case, if the system is invariant under time reversal, the elements of H are quaternion real. Otherwise, they are complex. This classification establishes four new random matrix ensembles [251, 33]. The microscopic spectral correlations of these ensembles are identical to those of the chiral ensembles if the parameters (the Dyson index β and the number of massless flavors N_f) are chosen appropriately.

7.6 Mathematical Physics and Quantum Gravity

RMT has received a great deal of attention as a problem in mathematical physics. We mention the relation between universal behavior in RMT and the asymptotic behavior of orthogonal polynomials [42, 43, 65, 252, 253], the relation between the classification of random matrix ensembles and the Cartan classification of symmetric spaces [34], and the theory of Riemannian superspaces [34]. Various methods for the solution of random matrix problems have been proposed. We mention the mapping to a gas of noninteracting fermions, the Coulomb gas method [27], the Brownian motion method [27], the replica method [107], the

orthogonal polynomial method [17], the supersymmetric method [102], and the operator method [177].

Generally, the problem for $\beta = 2$ is much simpler than for $\beta = 1$ and $\beta = 4$. Nevertheless, a great deal of progress has been made for $\beta = 1$ and $\beta = 4$. We mention relations between the kernels of the correlation functions [47, 48, 82, 83] and the relation between massless and massive correlators [85]. Novel mathematical methods have been developed for $\beta = 1$ and $\beta = 4$. We mention only the skew-orthogonal polynomial method [254, 255, 43, 47] and the extension of an operator method for $\beta = 2$ [81, 256, 82].

There exists an elaborate literature on the random matrix formulation of $2-d$ quantum gravity (see e.g. the recent reviews by Abdalla et al. [178] and Di Francesco et al. [177]). The idea is that the partition function, which is a sum over all metrics, can be rewritten as a sum over random surfaces. The sum over the dual graphs of a discretization of these random surfaces can be rewritten in terms of a random matrix partition function that can be analyzed with standard random matrix methods.

8 CONCLUSIONS

Chiral random matrix theory is the archetypal model for the spontaneous breaking of chiral symmetry. In chRMT, chiral symmetry is spontaneously broken for any finite number of massless flavors, whereas in QCD, breaking is believed to occur only below a certain number of massless flavors, perhaps as few as four. In this review, we have studied chiral symmetry breaking from the perspective of the eigenvalues of the QCD Dirac operator, where broken chiral symmetry implies that the smallest eigenvalues are spaced as $1/V$. The robustness of chiral symmetry breaking in chRMT can then be understood as the crystallization of the eigenvalues by the long-range random interactions. The number of eigenvalues in a sequence containing N eigenvalues fluctuates on average only by $\sqrt{\log N}/\pi$ as opposed to \sqrt{N} for uncorrelated eigenvalues. For uncorrelated eigenvalues, we do not expect chiral symmetry breaking for any number of massless flavors. The conclusion is that chiral symmetry breaking in QCD requires strongly correlated Dirac eigenvalues but not quite as strongly correlated as in chRMT. To make this conclusion more quantitative, we have formulated an effective theory for the QCD Dirac spectrum, which, in addition to the usual Goldstone modes, contains Goldstone bosons of spectral quarks that are “ghost” quarks introduced to probe the Dirac spectrum. Like the usual chiral Lagrangian, this Lagrangian consists of a kinetic term and a mass term. An important scale is the spectral mass for which the long-wavelength fluctuations of these two terms are of equal order of magnitude. In the theory of disordered condensed matter systems, this scale is known as the Thouless energy. For spectral masses below the Thouless energy, the mass dependence is given by the zero-momentum sector of the effective theory, and it coincides with that of chRMT in the limit of large matrices. The deviations from chRMT, given by the contributions of the nonzero-momentum modes, increase the fluctuations of the eigenvalues. For an increasing number of flavors, the position of the smallest eigenvalues moves to the right, whereas the slope of the spectral density increases with N_f . However, chiral symmetry remains broken for any value of N_f . The chiral condensate is simply a parameter of the effective partition function.

The statistical properties of the QCD Dirac eigenvalues have been investigated by numerous lattice QCD simulations, and the chRMT predictions have been verified in great detail. The behavior of Dirac spectra in the domain beyond the Thouless energy has been less well studied, but in all cases, the predictions of the effective theory for the Dirac spectrum agree well with lattice simulations.

Inspired by the successes of chRMT as an exact description of the statistical properties of the QCD Dirac spectrum, we have constructed a schematic model for the chiral phase transition. Although this approach does not provide rigorous results, it has been useful in advancing a qualitative understanding of the chiral phase transition at both zero and nonzero chemical potential. Examples are the properties of the Dirac spectrum in the approach to the critical temperature, the failure of the quenched approximation at $\mu > 0$, and the phase diagram of the QCD partition function in the $\mu T m$ plane.

Finally, RMT encapsulates a duality between order and chaos. Complete mixing of all degrees of freedom can be described by a single effective degree of freedom. This is the progress we have made toward an understanding of the complexity of the QCD vacuum.

Acknowledgments

This work was supported in part by the US Department of Energy under contracts DE-FG-88ER40388, DE-FG02-91ER40608, and DE-AC02-98CH10886. We would like to acknowledge discussions and collaborations on the subject of this review with G. Akemann, I.L. Aleiner, Y. Alhassid, A. Altland, B.L. Altshuler, M.E. Berbenni-Bitsch, B.A. Berg, D. Dalmazi, P.H. Damgaard, Y.V. Fyodorov, A.M. Garcia-Garcia, M. Göckeler, T. Guhr, M.Á. Halász, H. Hehl, A.D. Jackson, N. Kaiser, B. Klein, J.-Z. Ma, H. Markum, S. Meyer, S.M. Nishigaki, J.C. Osborn, R. Pullirsch, P.E.L. Rakow, A. Schäfer, M. Schnabel, A. Schwenk, B. Seif, T.H. Seligman, M.K. Şener, B.D. Simons, R.E. Shrock, E.V. Shuryak, A.V. Smilga, M.A. Stephanov, D. Toublan, H.A. Weidenmüller, T. Wilke, and M. Zirnbauer. We also thank I.L. Aleiner for a critical reading of Sec. 7.

Literature Cited

1. M. Gell-Mann and M. Lévy, *Nuovo Cim.* 16 (1960) 705.
2. B.W. Lee, *Chiral Dynamics* (Gordon and Breach, New York, 1972).
3. J. Goldstone, *Nuovo Cim.* 19 (1961) 154.
4. C. DeTar, *Quark-gluon plasma in numerical simulations of QCD*, in *Quark gluon plasma 2*, R. Hwa ed. (World Scientific, Singapore, 1995) p. 1.
5. E.V. Shuryak, *Nucl. Phys. B* 203 (1982) 93; E.V. Shuryak and J.J.M. Verbaarschot, *Nucl. Phys. B* 341 (1990) 1; D.I. Diakonov and V.Y. Petrov, *Nucl. Phys. B* 272 (1986) 457; T. Schäfer and E. Shuryak, *Rev. Mod. Phys.* 70 (1998) 323.
6. S. Weinberg, *Phys. Rev. Lett.* 18 (1967) 188; *Phys. Rev.* 166 (1968) 1568; *Physica A* 96 (1979) 327.
7. J. Gasser and H. Leutwyler, *Ann. Phys.* 158 (1984) 142; *Nucl. Phys. B* 250 (1985) 465; H. Leutwyler, *Ann. Phys.* 235 (1994) 165.
8. E.V. Shuryak, *Nucl. Phys. B* 302 (1988) 599; D.I. Diakonov and V.Y. Petrov, *Sov. Phys. JETP* 62 (1985) 204; D.I. Diakonov, hep-ph/9602375.
9. A.V. Smilga, *Phys. Rep.* 291 (1997) 1.
10. F. Karsch, *Nucl. Phys. B (Proc. Suppl.)* 83-84 (2000) 14.
11. D.T. Son, *Phys. Rev. D* 59 (1999) 094019.
12. M. Alford, K. Rajagopal, and F. Wilczek, *Phys. Lett. B* 422 (1998) 247; *Nucl. Phys. B* 537 (1999) 443.

13. R. Rapp, T. Schäfer, E.V. Shuryak, and M. Velkovsky, Phys. Rev. Lett. 81 (1998) 53; Ann. Phys. (NY) 280 (2000) 35.
14. J. Wishart, Biometrika 20 (1928) 32.
15. E.P. Wigner, Ann. Math. 53 (1951) 36.
16. C.E. Porter, *Statistical Theory of Spectra: Fluctuations* (Academic Press, New York 1965).
17. M. Mehta, *Random Matrices* (Academic Press, San Diego, 1991).
18. T. Guhr, A. Müller-Groeling, and H.A. Weidenmüller, Phys. Rep. 299 (1998) 189.
19. J. Gasser and H. Leutwyler, Phys. Lett. B 188 (1987) 477.
20. E.V. Shuryak and J.J.M. Verbaarschot, Nucl. Phys. A 560 (1993) 306.
21. C. Vafa and E. Witten, Nucl. Phys. B 234 (1984) 173.
22. M.E. Peskin, Nucl. Phys. B 175 (1980) 197; S. Dimopoulos, Nucl. Phys. B 168 (1980) 69; M.I. Vysotsky, Y.I. Kogan, and M.A. Shifman, Sov. J. Nucl. Phys. 42 (1985) 318.
23. H. Leutwyler and A.V. Smilga, Phys. Rev. D 46 (1992) 5607.
24. J.J.M. Verbaarschot, Phys. Rev. Lett. 72 (1994) 2531.
25. A. Smilga and J.J.M. Verbaarschot, Phys. Rev. D 51 (1995) 829.
26. D. Toublan and J.J.M. Verbaarschot, Nucl. Phys. B 560 (1999) 259.
27. F.J. Dyson, J. Math. Phys. 3 (1962) 140, 157, 166, 1199.
28. S.J. Hands and M. Teper, Nucl. Phys. B 347 (1990) 819.
29. T. Banks and A. Casher, Nucl. Phys. B 169 (1980) 103.
30. P. Hernandez, K. Jansen, and L. Lellouch, Phys. Lett. B 469 (1999) 198; Nucl. Phys. B (Proc. Suppl.) 83-84 (2000) 633.
31. A.V. Smilga, hep-th/9503049.
32. M.A. Nowak, J.J.M. Verbaarschot, and I. Zahed, Phys. Lett. B 217 (1989) 157; Y.A. Simonov, Phys. Rev. D 43 (1991) 3534.
33. A. Altland and M.R. Zirnbauer, Phys. Rev. Lett. 76 (1996) 3420; Phys. Rev. B 55 (1997) 1142.
34. M.R. Zirnbauer, J. Math. Phys. 37 (1996) 4986; F.J. Dyson, Commun. Math. Phys. 19 (1970) 235.
35. J.J.M. Verbaarschot, hep-th/9710114.
36. T. Akuzawa and M. Wadati, J. Phys. Soc. Jap. 67 (1998) 2151.
37. M.Á. Halász and J.J.M. Verbaarschot, Phys. Rev. D 52 (1995) 2563.
38. E. Witten, Ann. Phys. 128 (1980) 363.
39. R.A. Janik, M.A. Nowak, G. Papp, and I. Zahed, Nucl. Phys. B 498 (1997) 313.
40. I. Halperin and A. Zhitnitsky, Phys. Rev. Lett. 81 (1998) 4071.
41. P.H. Damgaard, Nucl. Phys. B 556 (1999) 327.
42. D. Fox and P.B. Kahn, Phys. Rev. 134 (1964) B1151.
43. T. Nagao and M. Wadati, J. Phys. Soc. Jap. 60 (1991) 3298; J. Phys. Soc. Jap. 61 (1992) 78, 1910.
44. F.J. Dyson and M. Mehta, J. Math. Phys. 4 (1963) 701.
45. J.J.M. Verbaarschot and I. Zahed, Phys. Rev. Lett. 70 (1993) 3852.
46. C.A. Tracy and H. Widom, Commun. Math. Phys. 161 (1994) 289.
47. J.J.M. Verbaarschot, Nucl. Phys. B 426 (1994) 559.
48. T. Nagao and P.J. Forrester, Nucl. Phys. B 435 (1995) 401.
49. E. Brézin, S. Hikami, and A. Zee, Nucl. Phys. B 464 (1996) 411.
50. J.J.M. Verbaarschot, Nucl. Phys. B 427 (1994) 534.
51. J.C. Osborn, D. Toublan and J.J.M. Verbaarschot, Nucl. Phys. B 540 (1999) 317.
52. P.H. Damgaard, J.C. Osborn, D. Toublan, and J.J.M. Verbaarschot, Nucl. Phys. B 547 (1999) 305.
53. A.V. Andreev, B.D. Simons, and N. Taniguchi, Nucl. Phys. B 432 (1994) 487.
54. P.H. Damgaard, Phys. Lett. B 424 (1998) 322; G. Akemann and P.H. Damgaard, Nucl. Phys. B 528 (1998) 411; Nucl. Phys. B 576 (2000) 597. P.H. Damgaard, hep-th/9807026.
55. G. Akemann and P.H. Damgaard, Phys. Lett. B 432 (1998) 390.
56. G. Akemann, P.H. Damgaard, U. Magnea, and S. Nishigaki, Nucl. Phys. B 487 (1997) 721.
57. E. Kanzieper and V. Freilikher, Phys. Rev. Lett. 78 (1997) 3806; Phys. Rev. E 55 (1997) 3712; *Diffuse Waves in Complex Media*, ed. J. P. Fouque, NATO ASI, Series C (Kluwer, Dordrecht, 1999) p. 165 (cond-mat/9809365).
58. S.M. Nishigaki, P.H. Damgaard, and T. Wettig, Phys. Rev. D 58 (1998) 087704.
59. P.H. Damgaard and S.M. Nishigaki, Phys. Rev. D 57 (1998) 5299.
60. J. Feinberg and A. Zee, J. Stat. Phys. 87 (1997) 473.

61. K. Splittorff, Nucl. Phys. B 548 (1999) 613.
62. K. Splittorff and A.D. Jackson, hep-lat/9805018.
63. M.J. Bowick and E. Brézin, Phys. Lett. B 268 (1991) 21.
64. J. Ambjørn, J. Jurkiewicz, and Y.M. Makeenko, Phys. Lett. B 251 (1990) 517.
65. E. Brézin and A. Zee, Nucl. Phys. B 402 (1993) 613.
66. C.W.J. Beenakker, Phys. Rev. Lett. 70 (1993) 1155.
67. G. Hackenbroich and H.A. Weidenmüller, Phys. Rev. Lett. 74 (1995) 4118.
68. V. Freilikher, E. Kanzieper, and I. Yurkevich, Phys. Rev. E 53 (1996) 2200.
69. V. Freilikher, E. Kanzieper, and I. Yurkevich, Phys. Rev. E 54 (1996) 210.
70. G. Akemann, Nucl. Phys. B 507 (1997) 475.
71. S. Higuchi, C. Itoi, S.M. Nishigaki, and N. Sakai, Phys. Lett. B 398 (1997) 123.
72. P. Zinn-Justin, Nucl. Phys. B 497 (1997) 725.
73. B. Eynard, Nucl. Phys. B 506 (1997) 633.
74. G. Akemann and J. Ambjørn, J. Phys. A 29 (1996) L555; G. Akemann and G. Vernizzi, hep-th/0002148; G. Akemann, G.M. Cicuta, L. Molinari, and G. Vernizzi, Phys. Rev. E 60 (1999) 5287; G. Akemann, Nucl. Phys. B 482 (1996) 403.
75. A.D. Jackson, M.K. Şener, and J.J.M. Verbaarschot, Nucl. Phys. B 479 (1996) 707.
76. A.D. Jackson, M.K. Şener, and J.J.M. Verbaarschot, Nucl. Phys. B 506 (1997) 612.
77. T. Guhr and T. Wettig, Nucl. Phys. B 506 (1997) 589.
78. E. Brézin and S. Hikami, Phys. Rev. E 56 (1997) 264.
79. B. Seif, T. Wettig, and T. Guhr, Nucl. Phys. B 548 (1999) 475.
80. P. Zinn-Justin, Commun. Math. Phys. 194 (1998) 631.
81. E. Brézin and H. Neuberger, Nucl. Phys. B 350 (1991) 513.
82. M.K. Şener and J.J.M. Verbaarschot, Phys. Rev. Lett. 81 (1998) 248.
83. H. Widom, J. Stat. Phys. 94 (1999) 347.
84. B. Klein and J.J.M. Verbaarschot, hep-th/0004119.
85. G. Akemann and E. Kanzieper, hep-th/0001188.
86. P.J. Forrester, T. Nagao, and G. Honner, Nucl. Phys. B 553 (1999) 601.
87. G. Akemann, P.H. Damgaard, U. Magnea, and S.M. Nishigaki, Nucl. Phys. B 519 (1998) 682.
88. E. Brézin and S. Hikami, Phys. Rev. E 57 (1998) 4140.
89. R.A. Janik, M.A. Nowak, G. Papp, and I. Zahed, Phys. Lett. B 446 (1999) 9.
90. R.C. Brower, P. Rossi, and C-I. Tan, Nucl. Phys. B 190 (1981) 699; R.C. Brower and M. Nauenberg, Nucl. Phys. B 180 (1981) 221.
91. F.A. Berezin and F.I. Karpelevich, Doklady Akad. Nauk SSSR 118 (1958) 9.
92. T. Guhr and T. Wettig, J. Math. Phys. 37 (1996) 6395.
93. A.D. Jackson, M.K. Şener and J.J.M. Verbaarschot, Phys. Lett. B 387 (1996) 355.
94. J.J.M. Verbaarschot, Phys. Lett. B 329 (1994) 351.
95. P.H. Damgaard, Phys. Lett. B 425 (1998) 151.
96. K. Zybalyuk, JHEP 6 (2000) 025.
97. F. Farchioni, hep-lat/9902029.
98. S. Descotes and J. Stern, hep-ph/9912234.
99. J.J.M. Verbaarschot, in *Continuous Advances in QCD*, Minneapolis 1994, A.V. Smilga ed. (World Scientific, Singapore, 1994) sp. 195 (hep-th/9405006).
100. A. Morel, J. Phys. France I 48 (1987) 1111.
101. E. Brézin, Lec. Notes Phys. 216 (1984) 115.
102. K.B. Efetov, Adv. Phys. 32 (1983) 53; *Supersymmetry in disorder and chaos* (Cambridge University Press, Cambridge, 1997).
103. J.J.M. Verbaarschot, H.A. Weidenmüller, and M.R. Zirnbauer, Phys. Rep. 129 (1985) 367.
104. C.W. Bernard and M.F.L. Golterman, Phys. Rev. D 49 (1994) 486; Nucl. Phys. B (Proc. Suppl.) 34 (1994) 331; M.F.L. Golterman, Acta Phys. Polon. B 25 (1994) 1731.
105. S. Sharpe, Phys. Rev. D 46 (1992) 3146.
106. M.F.L. Golterman and K.C. Leung, Phys. Rev. D 57 (1998) 5703.
107. S.F. Edwards and P.W. Anderson, J. Phys. F5 (1975) 965.
108. J.J.M. Verbaarschot and M.R. Zirnbauer, Ann. Phys. 158 (1984) 78.
109. P.H. Damgaard and K. Splittorff, Nucl. Phys. B 572 (2000) 478. P.H. Damgaard, Phys. Lett. B 476 (2000) 465. P.H. Damgaard and K. Splittorff, hep-lat/0003017.
110. A. Kamenev and M. Mezard, J. Phys. A 32 (1999) 4373; Phys. Rev. B 60 (1999) 3944.
111. I.V. Yurkevich and I.V. Lerner, Phys. Rev. B 60 (1999) 3955.

112. E. Kanzieper, cond-mat/9908130.
113. J.J.M. Verbaarschot and M.R. Zirnbauer, J. Phys. A 18 (1985) 1093.
114. M.R. Zirnbauer, cond-mat/9903338.
115. D. Dalmazi and J.J.M. Verbaarschot, hep-th/0005229 .
116. J.J.M. Verbaarschot, Phys. Lett. B 368 (1996) 137.
117. J.J.M. Verbaarschot, in *Nonperturbative Approaches to Quantum Chromodynamics*, D.I. Diakonov, ed., Gatchina 1995, p. 154.
118. A. Altland and B.D. Simons, Nucl. Phys. B 562 (1999) 445.
119. R. Gade and F. Wegner, Nucl. Phys. B 360 (1991) 213; R. Gade, Nucl. Phys. B 398 (1993) 499.
120. K. Takahashi and S. Iida, Nucl. Phys. B 573 (2000) 685.
121. T. Guhr, T. Wilke, and H.A. Weidenmüller, hep-th/9910107.
122. A. Smilga and J. Stern, Phys. Lett. B 318 (1993) 531.
123. J.J.M. Verbaarschot, Acta Phys. Polon. B 25 (1994) 133.
124. G.W. Carter and A.D. Jackson, Phys. Rev. D 61 (2000) 077902.
125. J.J.M. Verbaarschot and I. Zahed, Phys. Rev. Lett. 73 (1994) 2288.
126. C. Hilmoine and R. Niclasen, hep-th/0004081.
127. U. Magnea, Phys. Rev. D 61 (2000) 056005; Phys. Rev. D 62 (2000) 016005.
128. T. Nagao and S. M. Nishigaki, hep-th/0005077.
129. J. Christiansen, Nucl. Phys. B 547 (1999) 329.
130. P.H. Damgaard, U.M. Heller, A. Krasnitz, and T. Madsen, Phys. Lett. B 440 (1998) 129.
131. O. Bohigas and M.-J. Giannoni, *Lecture Notes in Physics* 209 (Springer, Berlin, 1984) 1.
132. A. Pandey, Ann. Phys. 134 (1981) 110.
133. Z. Pluhař and H. A. Weidenmüller, Phys. Rev. Lett. 84 (2000) 2833.
134. T.A. Brody, J. Flores, J.B. French, P.A. Mello, A. Pandey, and S.S.M. Wong, Rev. Mod. Phys. 53 (1981) 385; J. Flores, M. Horoi, M. Müller, and T.H. Seligman, cond-mat/0006144.
135. T. Guhr, J.-Z. Ma, S. Meyer, and T. Wilke, Phys. Rev. D 59 (1999) 054501.
136. A. Andersen, A.D. Jackson, and H.J. Pedersen, Nucl. Phys. A 650 (1999) 213.
137. J.C. Osborn and J.J.M. Verbaarschot, Phys. Rev. Lett. 81 (1998) 268; Nucl. Phys. B 525 (1998) 738.
138. U. Sharan and M. Teper, Phys. Rev. D 60 (1999) 054501; hep-ph/9910216; U. Sharan, hep-lat/9910038.
139. K.G. Wilson, Phys. Rev. D 10 (1974) 2445. A comprehensive reference is I. Montvay and G. Münster, *Quantum Fields on a Lattice* (Cambridge University Press, Cambridge, 1994).
140. H.B. Nielsen and M. Ninomiya, Nucl. Phys. B 185 (1981) 20; Nucl. Phys. B 193 (1981) 173.
141. P.H. Ginsparg and K.G. Wilson, Phys. Rev. D 25 (1982) 2649.
142. H. Neuberger, Phys. Lett. B 417 (1998) 141; Phys. Lett. B 427 (1998) 353; R. Narayanan and H. Neuberger, Phys. Rev. Lett. 71 (1993) 3251; Nucl. Phys. B 412 (1994) 574; Nucl. Phys. B 443 (1995) 305.
143. D.B. Kaplan, Phys. Lett. B 288 (1992) 342; Y. Shamir, Nucl. Phys. B 406 (1993) 90; V. Furman and Y. Shamir, Nucl. Phys. B 439 (1995) 54.
144. P. Hasenfratz, Nucl. Phys. B 525 (1998) 401; P. Hasenfratz and F. Niedermeyer, Nucl. Phys. B 414 (1994) 785.
145. H. Hehl and A. Schäfer, Phys. Rev. D 59 (1999) 117504.
146. J. Cullum and R.A. Willoughby, J. Comp. Phys. 44 (1981) 329.
147. T. Kalkreuter, Phys. Rev. D 51 (1995) 1305; Comput. Phys. Commun. 95 (1996) 1.
148. M.Á. Halász and J.J.M. Verbaarschot, Phys. Rev. Lett. 74 (1995) 3920; M.Á. Halász, T. Kalkreuter, and J.J.M. Verbaarschot, Nucl. Phys. B (Proc. Suppl.) 53 (1997) 266.
149. J.J.M. Verbaarschot, Nucl. Phys. B (Proc. Suppl.) 53 (1997) 88.
150. R. Pullirsch, K. Rabitsch, T. Wettig, and H. Markum, Phys. Lett. B 427 (1998) 119.
151. B.A. Berg, H. Markum, and R. Pullirsch, Phys. Rev. D 59 (1999) 097504.
152. R.G. Edwards, U.M. Heller, J. Kiskis, and R. Narayanan, Phys. Rev. Lett. 82 (1999) 4188.
153. S. Chandrasekharan and N. Christ, Nucl. Phys. B (Proc. Suppl.) 47 (1996) 527.
154. P.H. Damgaard, R.G. Edwards, U.M. Heller, and R. Narayanan, Phys. Rev. D 61 (2000) 094503; Nucl. Phys. B (Proc. Suppl.) 83-84 (2000) 434.
155. M.E. Berbenni-Bitsch, S. Meyer, A. Schäfer, J.J.M. Verbaarschot, and T. Wettig, Phys. Rev. Lett. 80 (1998) 1146.
156. J.-Z. Ma, T. Guhr, and T. Wettig, Eur. Phys. J. A 2 (1998) 87, 425.

157. P.H. Damgaard, U.M. Heller, and A. Krasnitz, Phys. Lett. B 445 (1999) 366.
158. M. Göckeler, H. Hehl, P.E.L. Rakow, A. Schäfer, and T. Wettig, Phys. Rev. D 59 (1999) 094503.
159. R.G. Edwards, U.M. Heller, and R. Narayanan, Phys. Rev. D 60 (1999) 077502.
160. J. Jurkiewicz, M.A. Nowak, and I. Zahed, Nucl. Phys. B 478 (1996) 605; Erratum Nucl. Phys. B 513 (1998) 759.
161. P.H. Damgaard and S.M. Nishigaki, Nucl. Phys. B 518 (1998) 495.
162. T. Wilke, T. Guhr, and T. Wettig, Phys. Rev. D 57 (1998) 6486.
163. T. Nagao and S.M. Nishigaki, hep-th/0001137; hep-th/0003009.
164. M.E. Berbenni-Bitsch, S. Meyer, and T. Wettig, Phys. Rev. D 58 (1998) 071502.
165. F. Farchioni, I. Hip, C.B. Lang, and M. Wohlgenannt, Nucl. Phys. B 549 (1999) 364; Nucl. Phys. B (Proc. Suppl.) 73 (1999) 939.
166. M.E. Berbenni-Bitsch, A.D. Jackson, S. Meyer, A. Schäfer, J.J.M. Verbaarschot, and T. Wettig, Nucl. Phys. B (Proc. Suppl.) 63 (1998) 820.
167. J. Smit and J.C. Vink, Nucl. Phys. B 286 (1987) 485; Nucl. Phys. B 298 (1988) 557; Nucl. Phys. B 303 (1988) 36; J.C. Vink, Phys. Lett. B 212 (1988) 483.
168. P.H. Damgaard, U.M. Heller, R. Niclasen, and K. Rummukainen, Phys. Rev. D 61 (2000) 014501.
169. F. Farchioni, I. Hip, and C.B. Lang, Phys. Lett. B 471 (1999) 58; Nucl. Phys. B (Proc. Suppl.) 83-84 (2000) 482.
170. M. Schnabel and T. Wettig, hep-lat/9912057.
171. F. Farchioni, P. de Forcrand, I. Hip, C.B. Lang, and K. Splittorff, Phys. Rev. D 62 (2000) 014503.
172. P.H. Damgaard, U.M. Heller, R. Niclasen, and K. Rummukainen, hep-lat/0003021.
173. A.M. Garcia-Garcia and J.J.M. Verbaarschot, hep-th/0003159.
174. M.E. Berbenni-Bitsch, M. Göckeler, T. Guhr, A.D. Jackson, J.-Z. Ma, S. Meyer, A. Schäfer, H.A. Weidenmüller, T. Wettig, and T. Wilke, Phys. Lett. B 438 (1998) 14; M.E. Berbenni-Bitsch, M. Göckeler, S. Meyer, A. Schäfer, and T. Wettig, Nucl. Phys. B (Proc. Suppl.) 73 (1999) 605.
175. M.E. Berbenni-Bitsch, M. Göckeler, H. Hehl, S. Meyer, P.E.L. Rakow, A. Schäfer, and T. Wettig, Phys. Lett. B 466 (1999) 293; Nucl. Phys. B (Proc. Suppl.) 83-84 (2000) 974.
176. P.W. Anderson, Phys. Rev. 109 (1958) 1492.
177. P. Di Francesco, P. Ginsparg, and J. Zinn-Justin, Phys. Rep. 254 (1995) 1.
178. E. Abdalla, M.C.B. Abdalla, D. Dalmazi, and A. Zadra, *2D-Gravity in Non-Critical Strings*, Lecture Notes in Physics, vol. M20 (Springer, Berlin, 1994).
179. A.D. Jackson and J.J.M. Verbaarschot, Phys. Rev. D 53 (1996) 7223.
180. T. Wettig, A. Schäfer, and H.A. Weidenmüller, Phys. Lett. B 367 (1996) 28.
181. M.A. Stephanov, Phys. Lett. B 375 (1996) 249.
182. A. Zee, Nucl. Phys. B 474 (1996) 726.
183. M.Á. Halász, A.D. Jackson, R.S. Shrock, M.A. Stephanov, and J.J.M. Verbaarschot, Phys. Rev. D 58 (1998) 096007.
184. I.M. Barbour, N.E. Behlil, E. Dagotto, F. Karsch, A. Moreo, M. Stone, and H.W. Wyld, Nucl. Phys. B 275 (1986) 296; M.-P. Lombardo, J.B. Kogut, and D.K. Sinclair, Phys. Rev. D 54 (1996) 2303.
185. I.M. Barbour, S.E. Morrison, E.G. Klepfish, J.B. Kogut, and M.-P. Lombardo, Nucl. Phys. (Proc. Suppl.) A 60 (1998) 220.
186. M.A. Stephanov, Phys. Rev. Lett. 76 (1996) 4472.
187. B. Vanderheyden and A.D. Jackson, Phys. Rev. D 61 (2000) 076004.
188. B. Vanderheyden and A.D. Jackson, hep-ph/0003150.
189. M.Á. Halász, A.D. Jackson, and J.J.M. Verbaarschot, Phys. Lett. B 395 (1997) 293; Phys. Rev. D 56 (1997) 5140.
190. I.M. Barbour, A.J. Bell, M. Bernaschi, G. Salina, and A. Vladikas, Nucl. Phys. B 386 (1992) 683.
191. M.Á. Halász, J.C. Osborn, M.A. Stephanov, and J.J.M. Verbaarschot, Phys. Rev. D 61 (2000) 076005.
192. J. Feinberg and A. Zee, Nucl. Phys. B 504 (1997) 579; Nucl. Phys. B 501 (1997) 643.
193. M.Á. Halász, J.C. Osborn, and J.J.M. Verbaarschot, Phys. Rev. D 56 (1997) 7059.
194. R.A. Janik, M.A. Nowak, G. Papp, J. Wambach, and I. Zahed, Phys. Rev. E 55 (1997) 4100; R.A. Janik, M.A. Nowak, G. Papp and I. Zahed, Nucl. Phys. B 501 (1997) 603.

195. H. Matsuoka and M. Stone, Phys. Lett. B 136 (1984) 204.
196. N. Bilić and K. Demeterfi, Phys. Lett. B 212 (1988) 83.
197. E.-M. Ilgenfritz and J. Kripfganz, Z. Phys. C 29 (1985) 79; P.H. Damgaard, D. Hochberg, and N. Kawamoto, Phys. Lett. B 158 (1985) 239; P.H. Damgaard, N. Kawamoto, and K. Shigemoto, Nucl. Phys. B 264 (1986) 1; P.E. Gibbs, Phys. Lett. B 172 (1986) 53, B 182 (1986) 369; N. Bilic, K. Demeterfi, and B. Petersson, Nucl. Phys. B 377 (1992) 651.
198. R.A. Janik, M.A. Nowak, G. Papp and I. Zahed, Nucl. Phys. A 642 (1998) 191.
199. A. Gocksch, Phys. Rev. D 37 (1988) 1014.
200. V.L. Girko, *Theory of random determinants* (Kluwer Academic Publishers, Dordrecht, 1990).
201. J. Feinberg and A. Zee, Nucl. Phys. B 552 (1999) 599; Phys. Rev. E 59 (1999) 6433.
202. D. Toublan and J.J.M. Verbaarschot, hep-th/0001110.
203. J.B. Kogut, M.A. Stephanov, and D. Toublan, Phys. Lett. B 464 (1999) 183.
204. J.B. Kogut, M.A. Stephanov, D. Toublan, J.J.M. Verbaarschot, and A. Zhitnitsky, hep-ph/0001171.
205. D.T. Son and M.A. Stephanov, hep-ph/0005225.
206. Y.V. Fyodorov and H.-J. Sommers, JETP Lett. 63 (1996) 1026.
207. K.B. Efetov, Phys. Rev. Lett. 79 (1997) 491; Phys. Rev. B 56 (1997) 9630.
208. A.V. Kolesnikov and K.B. Efetov, cond-mat/0001263.
209. H. Markum, R. Pullirsch, and T. Wettig, Phys. Rev. Lett. 83 (1999) 484.
210. J. Ginibre, J. Math. Phys. 6 (1965) 440.
211. Y.V. Fyodorov, B.A. Khoruzhenko, and H.-J. Sommers, Phys. Lett. A 226 (1997) 46.
212. Y.V. Fyodorov, B.A. Khoruzhenko, and H.-J. Sommers, Phys. Rev. Lett. 79 (1997) 557.
213. P.J. Forrester, J. Phys. A 32 (1999) L159.
214. A. Barducci, R. Casalbuoni, S. De Curtis, R. Gatto, and G. Pettini, Phys. Lett. B 231 (1989) 463; Phys. Rev. D 41 (1990) 1610; Phys. Lett. B 301 (1993) 95; Phys. Rev. D 49 (1994) 426.
215. J. Berges and K. Rajagopal, Nucl. Phys. B 538 (1999) 215.
216. T. Schäfer, Phys. Rev. D 57 (1998) 3950.
217. C. Baillie, K.C. Bowler, P.E. Gibbs, I.M. Barbour, and M. Rafique, Phys. Lett. B 197 (1987) 195.
218. A.V. Kolesnikov and K.B. Efetov, Waves in Random Media 9 (1999) 71.
219. C.W.J. Beenakker, Rev. Mod. Phys. 69 (1997) 731.
220. G. Montambaux, in *Quantum Fluctuations, Les Houches, Session LXIII*, eds. E. Giacobino, S. Reynaud, and J. Zinn-Justin, Elsevier Science, 1995 (cond-mat/9602071).
221. M.A. Stephanov, J.J.M. Verbaarschot, and T. Wettig, in *Encyclopedia of Electrical and Electronics Engineering*, J. Webster, ed. (Wiley, New York, 2000).
222. A. Mironov, A. Morozov, and G. Semenoff, Int. J. Mod. Phys. A 11 (1996) 5031.
223. D. Gross and E. Witten, Phys. Rev. D 21 (1980) 446; E. Brézin and D. Gross, Phys. Lett. B 97 (1980) 120.
224. S. Chandrasekharan, Phys. Lett. B 395 (1997) 83.
225. T. Eguchi and H. Kawai, Phys. Rev. Lett. 48 (1982) 1063.
226. S.R. Das, Rev. Mod. Phys. 59 (1987) 235.
227. R. Dijkgraaf, hep-th/9201003.
228. I.K. Kostov, hep-th/9907060.
229. V.A. Kazakov and A.A. Migdal, Nucl. Phys. B 397 (1993) 214.
230. M. Moshe, H. Neuberger, and B. Shapiro, Phys. Rev. Lett. 73 (1994) 1497.
231. D.J. Thouless, Phys. Rep. 13 (1974) 93.
232. B.L. Altshuler and B.I. Shklovskii, Zh. Exp. Teor. Fiz. 91 (1986) 220 (Sov. Phys. JETP 64 (1986) 127).
233. S. Washburn and R.A. Webb, Adv. Phys. 35 (1986) 375.
234. D.R. Hofstadter, Phys. Rev. B 14 (1976) 2239.
235. K. Slevin and T. Nagao, Phys. Rev. Lett. 70 (1993) 635.
236. G. Parisi, J. Phys. A 14 (1981) 735.
237. M.E. Berbenni-Bitsch, private communication.
238. B.L. Altshuler, I.K. Zharekeshev, S.A. Kotochigova, and B.I. Shklovskii, Sov. Phys. JETP 67 (1988) 625.
239. A.J. McKane and M. Stone, Ann. Phys. (NY) 131 (1981) 36.
240. O. Bohigas, M. Giannoni, and C. Schmit, Phys. Rev. Lett. 52 (1984) 1.

241. T.H. Seligman, J.J.M. Verbaarschot, and M. Zirnbauer, Phys. Rev. Lett. 53 (1984) 215;
T.H. Seligman and J.J.M. Verbaarschot, Phys. Lett. A 108 (1985) 183.
242. T.S. Biro, S.G. Matinyan, and B. Müller, *Chaos and Gauge Field Theory*, World Scientific
Lecture Notes in Physics, Vol. 56 (1995).
243. K. Johnson, L. Lellouch, and J. Polonyi, Nucl. Phys. B 367 (1991) 675.
244. R.A. Janik, M.A. Nowak, G. Papp, and I. Zahed, Phys. Rev. Lett. 81 (1998) 264.
245. H.A. Weidenmüller, Nucl. Phys. A 518 (1990) 1.
246. T. Guhr and A. Müller-Groeling, J. Math. Phys. 38 (1997) 1870.
247. J. Miller and J. Wang, Phys. Rev. Lett. 76 (1996) 1461.
248. N. Hatano and D.R. Nelson, Phys. Rev. Lett. 77 (1996) 570.
249. P.W. Brouwer, P.G. Silvestrov, and C.W.J. Beenakker, Phys. Rev. B 56 (1997) 4333.
250. A.F. Andreev, Zh. Eksp. Teor. Fiz. 46 (1964) 1823.
251. R. Oppermann, Physica A 167 (1990) 301.
252. B. Eynard, Nucl. Phys. B 506 (1997) 633.
253. N. Deo, Nucl. Phys. B 504 (1997) 609; E. Brézin and N. Deo, Phys. Rev. E 59 (1999) 3901.
254. F. Dyson, J. Math. Phys. 13 (1972) 90.
255. G. Mahoux and M. Mehta, J. Phys. France I 8 (1991) 1093.
256. C.A. Tracy and H. Widom, J. Stat. Phys. 92 (1998) 809.